Skytruck Enterprises

Design of the Boomerang Military Flying Straddle Carrier

AIAA Undergraduate Individual Aircraft Design Competition 2015-2016

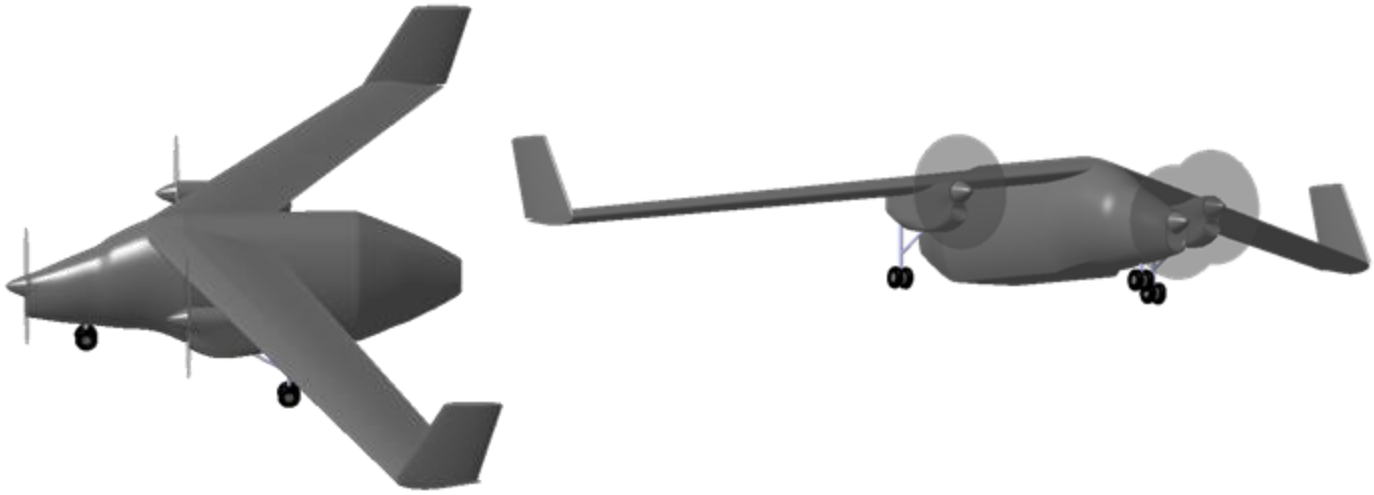

CAL POLY POMONA

California State Polytechnic University, Pomona

Department of Aerospace Engineering

Daniel Lucak

Advisor: Dr. Donald Edberg

Skytruck Enterprises

Chief Design Engineer

AIAA Number: 517952

Advisor: Dr. Donald Edberg

AIAA Number: 022972-00

Table of Contents

List of Symbols

Symbol	Description	Units
A_0	Cross-sectional Area	ft^2
AR	Aspect Ratio	-
b	Wingspan	ft
$\bar{c}$	Mean Aerodynamic Chord	ft
C_D	Drag Coefficient	-
C_{D_0}	Zero-Lift Drag Coefficient	-
C_F	Skin Friction Coefficient	-
C_l	Section Lift Coefficient	-
C_{l_β}	Roll Stability Derivative	1/radian
C_{l_p}	Roll Damping Derivative	1/radian
C_L	Wing Lift Coefficient	-
C_{L_α}	Lift Curve Slope	1/radian
C_m	Pitching Moment Coefficient	-
C_{M_q}	Pitch Damping Derivative	1/radian
C_{n_β}	Directional Stability Derivative	1/radian
$C_{n_{\delta_R}}$	Yawing Moment due to Rudder Derivative	1/radian
C_{y_β}	Side Force due to Sideslip Derivative	1/radian
$C_{y_{\delta_R}}$	Side Force due to Rudder Deflection Derivative	1/radian
c_p	Brake Specific Fuel Consumption	lb hp/hr
$C_{m,\alpha=0}$	Pitching Moment Coefficient at 0 Angle of Attack	-

e	Oswald Efficiency Factor	-
F	Fineness Ratio	-
F	Fuel Weight Flow Rate	lb/s
K	Form Factor Correction	-
K	Induced Drag Coefficient	-
M	Mach Number	-
n	Load Factor	-
P	Power	hp
P_A	Power Available	hp
q	Dynamic Pressure	psi, lb/ft
Re	Reynold's Number	-
R/C	Rate of Climb	ft/min
S	Surface Area	ft^2
S_w	Wing Area	ft^2
S_{wet}	Wetted Area	ft^2
t	Thickness	ft
T	Thrust	lb
T	Temperature	°R, °F
V	Velocity	ft/s, kt
w	Induced Velocity	ft/s, kt
W	Weight	lb
α	Angle of Attack	degrees
β	Sideslip Angle	degrees

δ_R	Rudder Deflection	degrees
η_b	Proportion of Wing Semi-Span Covered	-
λ	Taper Ratio	-
Λ	Sweep Angle	degrees
ρ	Density	sl/ft^3
σ	Crab Approach Angle	degrees

Acronym	**Description**	**Units**
AC	Aerodynamic Center	-
AIAA	American Institute of Aeronautics and Astronautics	-
APU	Auxiliary Power Unit	-
CBR	California Bearing Ratio	-
CG	Center of Gravity	-
CT	Conventional Tailless	-
MAC	Mean Aerodynamic Chord	ft
NACA	National Advisory Committee for Aeronautics	-
RFP	Request for Proposal	-
SBT	Single Boom Tail	-
SIT	Swift-Inspired Tailless	-
TBT	Twin Boom Tail	-

List of Figures

List of Tables

Compliance Matrix

RFP Requirement	Value	Capability	Section
Aircraft type	Fixed wing	Fixed Wing	2.0
Payload Weight	45,140 lb total	45,140 lb	5.2
Payload Location	External	External	5.2
Crew	3	3	5.1
Minimum cruise speed	250 kts	300 kt	16.0
Minimum cruise altitude	23,000 ft	>36,000 ft	16.0
Service ceiling with empty container	33,000 ft	41,000 ft	15.1
Rate of climb, max takeoff weight, 10,000 ft	1,500 ft/min	2,140 ft/min	15.1
Takeoff distance	3,500 ft	3,460 ft	21.1
Landing Distance	3,500 ft	3,370 ft	21.2
Range with full payload	1,000 nm	1,090 nm	20.0
Flight without container	Possible	Possible	5.2
Engine	Rolls-Royce Allison T-56-A-15	Rolls-Royce Allison T-56-A-15	12.0
Propeller	Hamilton Sundstrand NP2000	Hamilton Sundstrand NP2000	12.0
MILSPEC Requirement			
Fuel Reserves	30 min loiter +5% total	30 min loiter +5% total	16.1
Landing Thrust Reverse	Not considered for landing length	Not considered for landing length	21.2
Derived Requirements			
Container Loading System	Self-Contained	Self-Contained	5.2
Soft Field Performance	Operate from field with CBR ≤ 6	Min CBR = 4	22.4
C_{M_α} derivative	< 0	-0.27	19.1.6
C_{n_β} derivative	> 0	0.09	19.1.6
C_{l_p} derivative	< 0	-.422	19.1.6
C_{M_q} derivative	< 0	-2.7	19.1.6
C_{l_β} derivative	< 0	-0.26	19.1.6

The Skytruck Enterprises Boomerang Military Flying Straddle Carrier 3-View

Empty Weight	39,800 lb
MTOW	92,400 lb
Wing Area	1,350 ft^2
Fuel Weight (1,000 nm mission)	7,500 lb
Wingspan	116.2 ft
Prop Diameter	13.5 ft

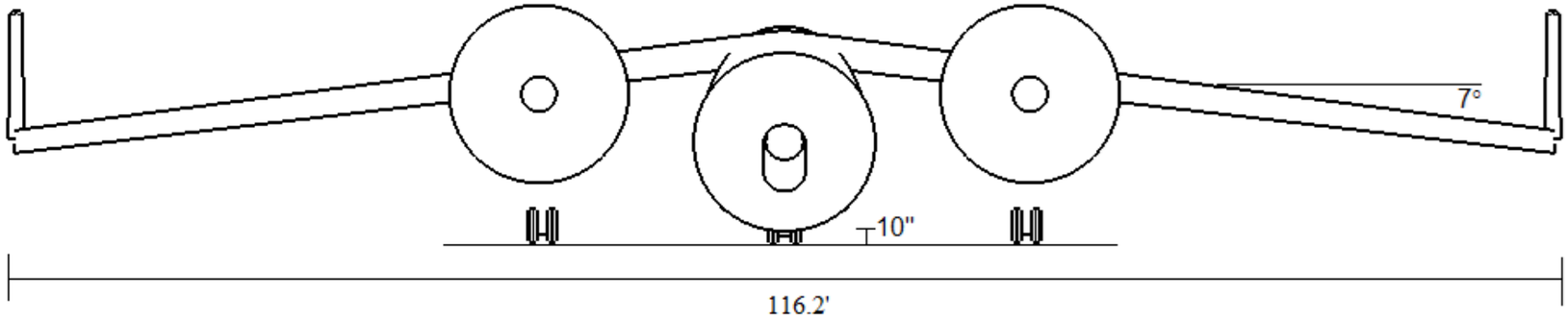

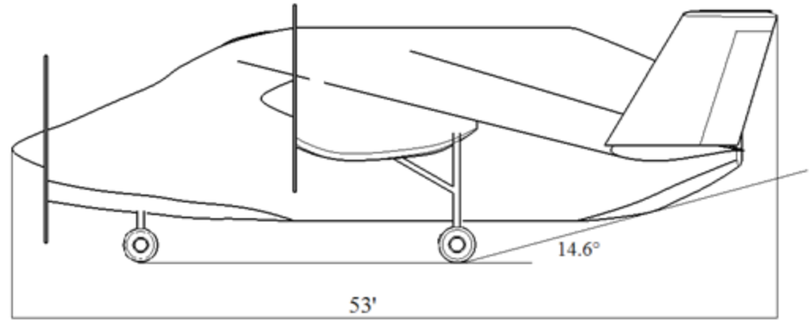

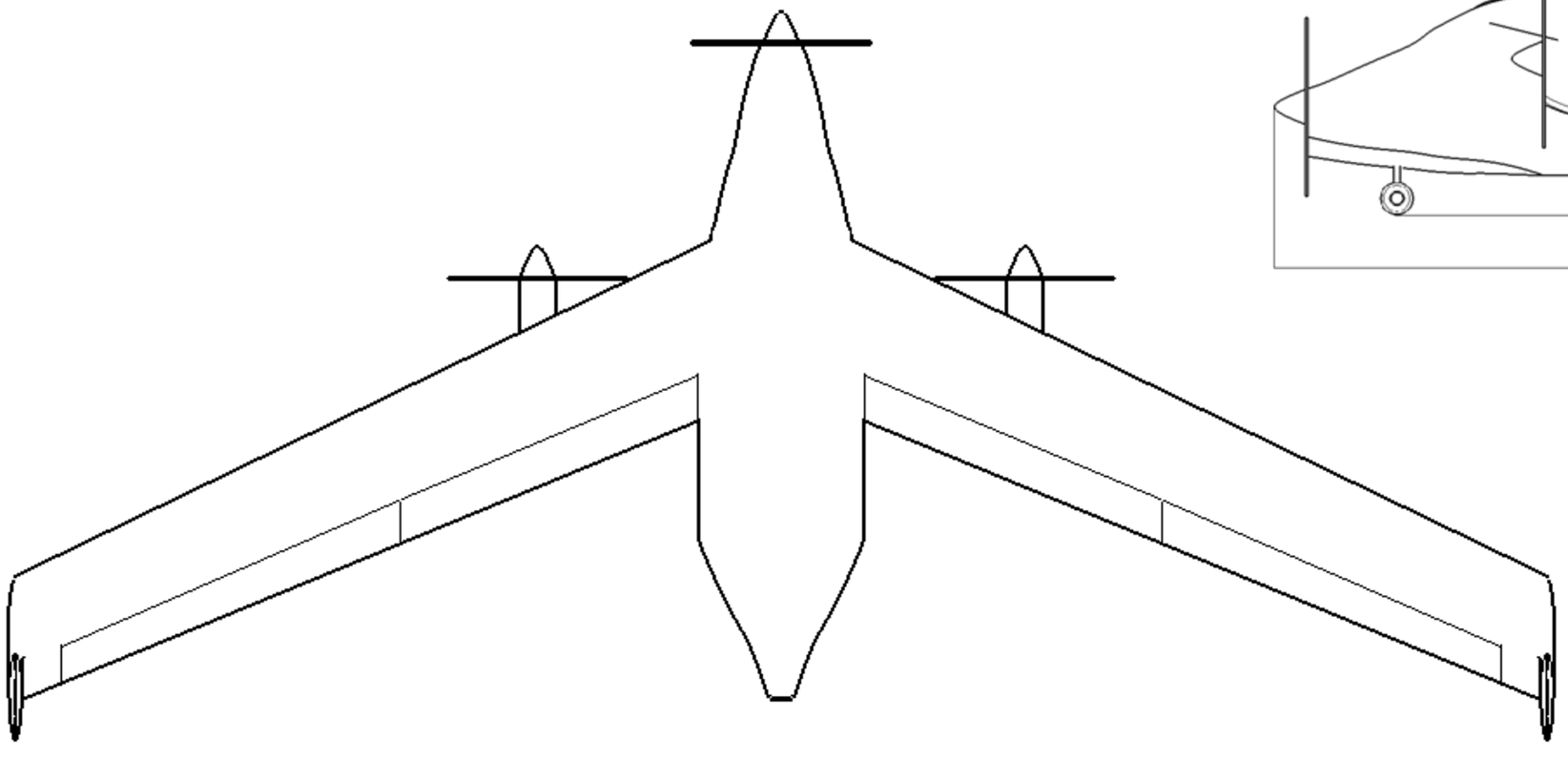

1.0 Introduction

The cargo fleets of military forces of the world boast a wide range of aircraft capable of delivering their payloads all over the world in time frames unimaginable even 75 years ago. Despite their reach and speed, fixed-wing cargo aircraft still have a number of limitations. Though the most obvious is a suitable runway, operating a cargo aircraft requires a great deal of specialized equipment operated by knowledgeable people. Cargo generally must also be loaded in specialized containers, usually various types of pallets, in order to be held in the cargo hold of the aircraft. In response, the American Institute of Aeronautics and Astronautics (AIAA) released a Request for Proposal (RFP) specifying a cargo aircraft able to operate in and out of austere fields able to carry an unmodified standard ISO 20' container. These containers are an ideal cargo for many reasons. They are ubiquitous and widely available around the world, able to carry a large volume of cargo, and flexible enough to be used not only as cargo containers but also temporary shelters or buildings. Though current systems such as the Lockheed C-130, Boeing C-17, and Lockheed C-5 are currently able to carry these containers, they require specialized equipment and loading procedures [1]. Thus, there is a need for an aircraft that can readily accept such a container and deliver it to an unprepared field.

Figure 1.0-1: ISO 20 ft Container loading of a C-130[1]

[1] http://www.cdkmobile.com/container_aircraft_loading.htm

1.1 Design Approach

With a very specific, well defined payload and an emphasis on speed and ease of loading and unloading, the design could be very well-tailored to the specific role. The design process began with a review of the RFP as part of a requirements analysis to determine the major derived requirements. A historical review of past and current aircraft was then performed as a starting point to determine possible design features. This historical review was ongoing throughout the whole design process as past aircraft were continually referenced to provide previous ideas of solutions, failures, and reasonable results of various design features. With the help of various aircraft design guides noted throughout the report and summarized in the References, several preliminary design architectures were developed. These were then down selected to two architectures that were analyzed more closely. From these two, a single final architecture was selected. With a single architecture, final analysis and design changes were implemented in an iterative fashion to produce the final design.

1.2 Design Tools

Along with Microsoft Office software used for the majority of the analysis, MATLAB and XFLR5 were both used to facilitate some aspects of the design. XFLR5 is an aerodynamic analysis tool that incorporates both 2D and 3D tools. Its 2D analysis capabilities are derived from earlier Xfoil codes, and the 3D analysis utilizes Lifting Line Theory, the Vortex Lattice Method, and the 3D Panel Method. With these analyses, the program can calculate aerodynamic coefficients as well as stability analyses.

1.3 Request for Proposal

Based on the preceding need, the RFP provided by the AIAA lists the following guidelines for the design of the Military Flying Straddle Carrier. Among the listed performance

requirements, the engines are specified as Rolls-Royce Allison T-56-A-15 turboprops mated with Hamilton Sundstrand NP2000 propellers. This is the propulsion system found on the U.S. Air Force C-130H and the Navy E-2 Hawkeye, thus maintaining commonality for parts and maintenance.

Table 1.3-1: Military Flying Straddle Carrier RPF Specifications

Basic Requirements	
Aircraft type	Fixed wing
Payload	One 20' ISO standard container • Empty weight: 5,140 lb • Maximum load in container: 40,000 lb • Must be external to the aircraft
Performance Requirements	
Crew	3
Cruise with maximum load	>250 kts >23,000 ft altitude
Service ceiling with empty container	33,000 ft
Rate of climb, max takeoff weight, 10,000 ft	1,500 ft/min
Takeoff and landing distances	3,500 ft
Range with full payload	1,000 nm
Other Considerations	
Engine	Rolls-Royce Allison T-56-A-15
Propeller	Eight bladed Hamilton Sundstrand NP2000

1.4 Other Requirements

In addition to the RFP requirements, U.S. military aircraft must also conform to the U.S. Military Standards, or MilSpecs. Many requirements as well as definitions are found in [2], MIL-C-005011B, which governs the performance of piloted, fixed-wing aircraft. Areas influenced by MilSpec standards will be noted throughout the report, and a summary can be found in the compliance matrix.

1.5 Mission Profile

From the previous requirements, two mission profiles were developed, one for the fully loaded container and one for an empty container. These mission profiles are very similar and

differ only during the cruise section. Both missions also take into account a reserve leg as specified in [2], which is a 30 minute loiter at conditions for max endurance.

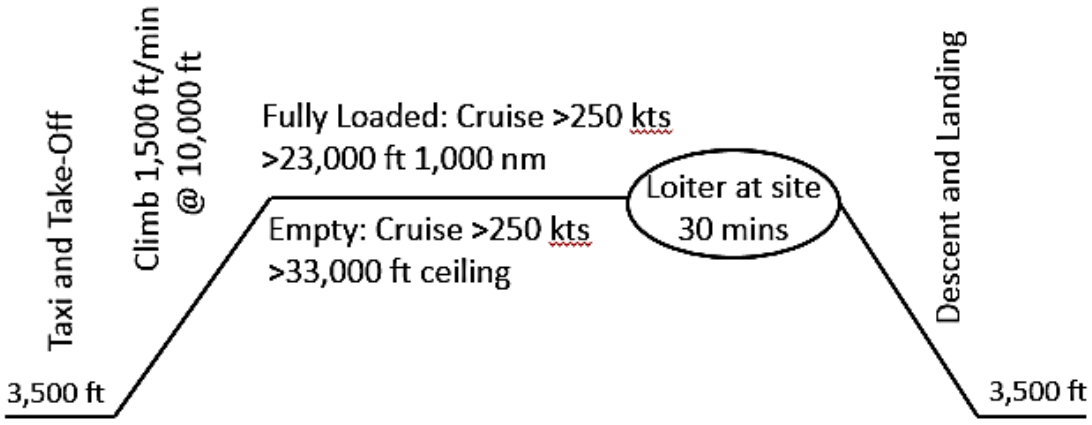

Figure 1.5-1: Mission Profile

1.6 Relevant Historical Aircraft

In the following report, several aircraft are referenced and served as starting points for research into particular aspects of the current design effort.

1.6.1 Lockheed C-130 Hercules

In production for over 50 years, the Lockheed C-130 is the mainstay of military forces around the world. Powered by four Allison T-56 turboprop engines, the same ones specified in the RFP, the C-130 has filled roles not only as a tactical airlifter capable of operating out of rough airfields, but also as an aerial refueling platform, a gunship, and an aerial firefighter, among others. This flexible airframe has a maximum payload of 45,000 pounds in a hold 40 ft long, 9 ft tall, and just under 10 ft wide. Thus, it can fit a 20 ft ISO container, but

Figure 1.6.1-1: C-130 demonstrating rough field operations[2]

[2] http://www.wvgazettemail.com/article/20140804/DM01/140809711/1298

extra equipment is required to load and secure it [1]. With a similar payload weight and identical engines, the C-130 is a logical starting point for the RFP to get an idea of the size and capabilities of the future design.

1.6.2 Fairchild XC-120 Packplane

Developed from the Fairchild C-119 Flying Boxcar, the XC-120 was the first aircraft, and the only one actually flown, designed around the "trailer-truck principle" of an aircraft with a quickly detachable, external cargo pod [3]. Though the idea did not gain acceptance, its concept of operations is very similar to the current design. It was envisioned that the pod could be loaded with any of a variety of items – "a command post, radar station, repair shop, or field hospital," for example – flown to the forward field of operations, quickly unloaded, and then flown back empty to pick up another pod [3]. The estimated max weight of the cargo was around 20,000 pounds, and the range was estimated to be roughly 2,260 miles. The pod itself is equipped with its own undercarriage and is hoisted onto the aircraft by means of electrical cable hoists to allow it to be quickly carted away. Since this was merely a test aircraft, it was hoped that a purpose-built cargo pod-carrying aircraft would gain popular traction, though this need never materialized.

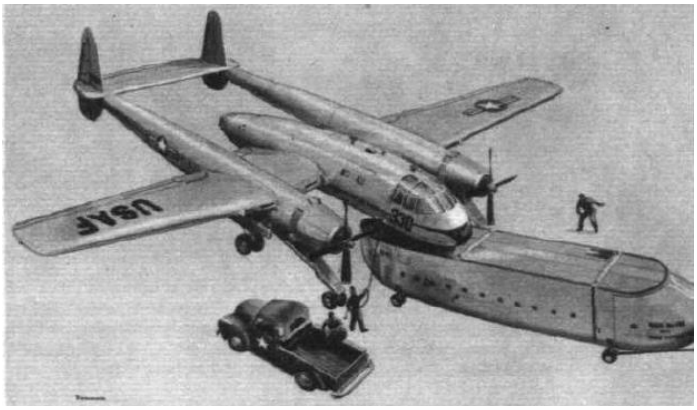

Figure 1.6.2-1: XC-120 pod operations [3]

1.6.3 Northrop YB-35

Figure 1.6.3-1: YB-35 with counterrotating turboprops[3]

A tailless configuration was studied early in the design process, and the advanced but operationally unsuccessful YB-35 was studied as an example of a large, tailless turboprop powered aircraft. The pinnacle of Jack Northrop's quest for a true flying wing, the YB-35, and its turbojet powered successor, the YB-49, were very advanced for their time. The turboprop-powered YB-35 could carry a load of bombs of over 50,000 pounds over a range greater than 8,000 miles. Though hampered by gearbox issues and some stability issues that were never entirely remedied, these large flying wings proved the viability of a tailless aircraft able to carry a large payload. When fully loaded, the aircraft had a wing loading of approximately 50 lb/ft^2.

1.6.4 Aériane Swift

The Swift is a rigid-winged, foot-launched, tailless sailplane originally designed by a team lead by Ilan Kroo. Unlike many tailless designs that have to employ airfoil sections with reflexed camber in order to maintain longitudinal stability and trim, the Swift employs a novel approach to longitudinal trim. With sufficient sweep and a carefully designed planform, the flap on the inboard section of the wing produces a lift force in

Figure 1.6.5-1: Swift hang glider in flight [4]

[3] http://www.avionslegendaires.net/avion-militaire/northrop-xb-35-yb-35/

front of the aircraft center of gravity, thus inducing a positive, nose-up pitching moment. Thus, the glider uses the inboard flap to trim in flight while also being able to extend it to increase both lift and drag for landing. Vertical surfaces on the wing tips also negate the need for complex drag-rudders. Though just a hang glider, these features can be scaled up to a much larger aircraft.

2.0 Concept of Operations

With the RFP and other requirements in mind, a concept of operations was developed in order to most effectively meet the mission specifications. With the specialized cargo and emphasis on rapid and simple unloading, the aircraft is designed to operate with a minimum of outside equipment, especially when unloading. A typical mission begins at a main base within 1,000 nm of a forward arena of operations. The container is brought to the aircraft with the help of a container mover, and it is loaded onto the aircraft. From the main base, the aircraft flies 1,000 nm or less to the forward arena, where an unimproved dirt runway may be the only runway available. After landing, the container can be directly lowered from the aircraft to the ground or to a container mover with no extra equipment. Another container could be loaded onto the aircraft, or it can return empty. The aircraft is then refueled and returns to its base.

3.0 Derived Requirements and Requirements Flowdown

Based on the concept of operations, a number of derived requirements were developed. These requirements and a justification are presented in Table 3.0-1.

Table 3.0-1: Derived requirements

Requirement	Justification
Self-contained container loading system	Allows containers to be unloaded with no outside equipment
Can lower container from aircraft to ground level	Allows containers to be unloaded with no outside equipment
High wing	Allows container to be vertically lowered directly to the ground
Operate from fields with a California Bearing Ratio (CBR) of 6 or less	Required for soft/unprepared field operations

With these requirements and the RFP requirements in mind, some basic characteristics common to any concept were defined in the requirements flow down.

3.1 Fuselage

Owing to the specific required payload, the potential architectures could be closely tailored to fit the particular mission. Of particular importance is the container's relatively short length at only 20 ft. For comparison, the C-130's cargo hold is 40 ft long; a single 20 ft container in this large hold would result in significant wasted, empty space. Thus, the current design does not require a very long fuselage. The fuselage length will only be taken up by the cockpit and forward streamlining, the container itself, and any aerodynamic fairing used aft of the container. The surfaces on the sides and bottom of the container will also be streamlined, but will not be load-carrying.

The lack of any load-bearing structure for the majority of the fuselage leads to the necessity of landing gear attachment point not directly connected to the fuselage. In previous designs, this has been accomplished by retracting the gear either into the engine pylon (as in the DHC-8) or into the wing (as in the B-24) for high wing aircraft.

In order to facilitate rapid unloading with no external equipment, a self-contained loading and lowering system integrated into the fuselage is required. This system must be able to operate with no external power and lower a container fully to ground level so that it can be unloaded anywhere that the aircraft can land.

3.2 Wing

In order to position the container under the fuselage for it to be loaded using the loading system, the aircraft requires a high wing. Since the container will make up a significant portion of the aircraft's loaded weight, its CG must be near the aircraft's empty CG, which in turn must

be near the aircraft's aerodynamic center for stability. Even with generous sweep, a portion of the container will still overlap most of the inboard wing, as shown in Figure 3.2-1. To unload the container vertically to the ground, this central overlap region must not contain any wing structural elements. Thus, the container must either translate horizontally during loading and unloading, adding complexity, or the wing cannot utilize a pass-through spar, again adding weight and sructural complexity. The much simpler solution is to utilize a high wing which also has the benefits of easing accessibility around the aircraft and increasing propeller clearance for wing-mounted engines.

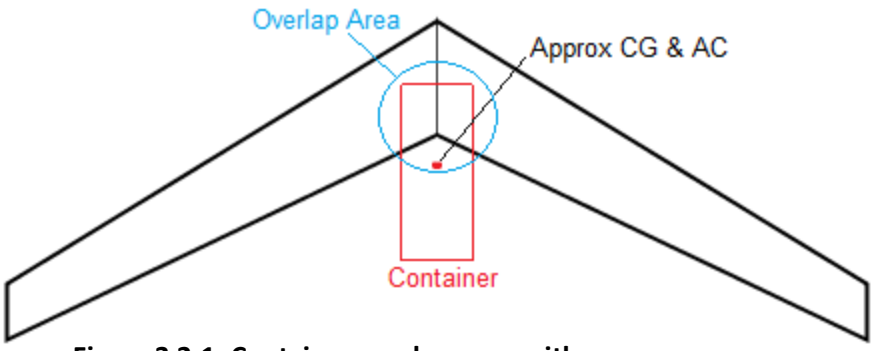

Figure 3.2-1: Container overlap even with generous sweep

3.3 Landing Gear and Related Systems

The landing gear and tires are the main components affected by the RFP requirement to land and take off on rough surfaces. One of the measures of an airfield's surface quality is California Bearing Ratio (CBR). Using this scale, a lower value correlates with a softer, less compacted surface. From Currey [5] a CBR of 6-9 is a typical value of a soft, unpaved airfield. Thus, operations on fields with a CBR of 6 is a derived requirement for the aircraft.

4.0 Architecture Down Select

4.1 Preliminary Architectures

Though the rather short, stubby fuselage is needed in the interest of efficient use of volume and minimization of wetted area, it creates a problem of locating the tail surfaces far enough aft of the center of gravity. With a moment arm too short, the tail surfaces would tend to

be very large, increasing wetted area and drag. Thus, four preliminary architecture concepts were developed – two with conventional tail surfaces, single boom and twin boom, and two tailless, conventional and Swift-inspired.

4.1.1 Twin Boom

Though generally falling out of favor, the twin boom concept was popular up until the early jet age. Among cargo and transport aircraft, the most prominent examples are the Fairchild C-82 Packet and the larger C-119 Flying Boxcar show in Figure 4.1.1-1. As evidenced by the XC-120, the twin boom configuration is well suited to the present mission. The tail structure is separated from the fuselage structure, so the fuselage does not need to be lengthened significantly beyond the payload length to provide an adequate moment arm for the tail surfaces. Its main drawback is the added weight and wetted area contributed by the booms themselves.

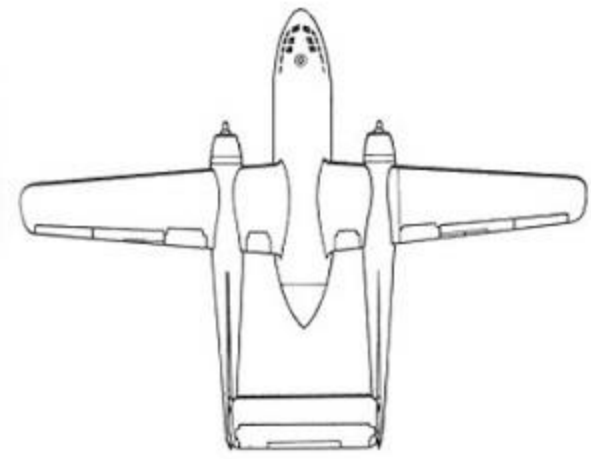

Figure 4.1.1-1: C-119 Top view showing twin boom configuration[4]

4.1.2 Single Boom

Though uncommon, a single tail boom captures the advantage of lengthening the tail arm while keeping the main fuselage length matched to the payload. It also reduces wetted area and weight compared to a twin boom

Figure 4.1.2-1: Blackburn Beverley heavy transport with a single tail boom[5]

[4] http://4.bp.blogspot.com/_rUHyHq68ak0/SLgJs0HOajI/AAAAAAAAQ-w/Pzflo3MAoYA/s400/c119-3view.jpg
[5] http://s104980574.websitehome.co.uk/ca/p2%20images/beverley9.jpg

configuration. The main drawback of a single boom configuration is the structural requirements of the boom itself. Whereas the twin boom utilizes widely spaced beams to greatly increase effective stiffness, the single boom would have to withstand the forces generated by the tail alone. The tail forces would induce bending in every direction as well as torsional loads, so a very robust structure would be required.

4.1.3 Conventional Tailless

For this mission, a tailless aircraft has the advantage of eliminating the tail surfaces altogether, again allowing the fuselage to conform to the payload. Though a tailless configuration is not conventional, per se, most tailless aircraft have a number of similar features. In order to trim at a positive angle of attack, reflex camber is required to produce a positive C_m at zero angle of attack. The addition of reflex camber both reduces lift at a particular angle of attack and reduces max C_L. Effective high lift devices are also not usable since the center of pressure for the flaps is behind the center of gravity. Thus, flap deflection to increase lift also induces a negative, nose-down pitching moment that may be impossible to trim. These combination of these two factors causes a traditional tailless aircraft to have a very low maximum C_L. Thus, large wing areas and high takeoff and landing speeds are required.

4.1.4 Swift-Inspired Tailless

Drawing on Kroo's design of the Swift in [4] as well as NACA TN837 [6], high lift devices can be incorporated into a tailless design. With properly implemented sweep, taper, and twist, the wing aerodynamic center can be moved far enough aft that the aircraft can be both stable and trimmable with conventional (non-reflex) airfoil sections. With sufficient sweep, the center of gravity can be placed ahead of the aerodynamic center, thus achieving static stability,

while an inboard flap can also induce a load forward of the center of gravity. This flap thus induces a positive, nose-up moment when deflected, allowing the aircraft to trim at any angle of attack. This concept is illustrated in NACA TN837, shown in Figure 4.1.4-1. This trim flap can be used to increase lift during takeoff and landing much like a traditional flap, allowing a smaller wing than would otherwise be possible without effective high lift devices.

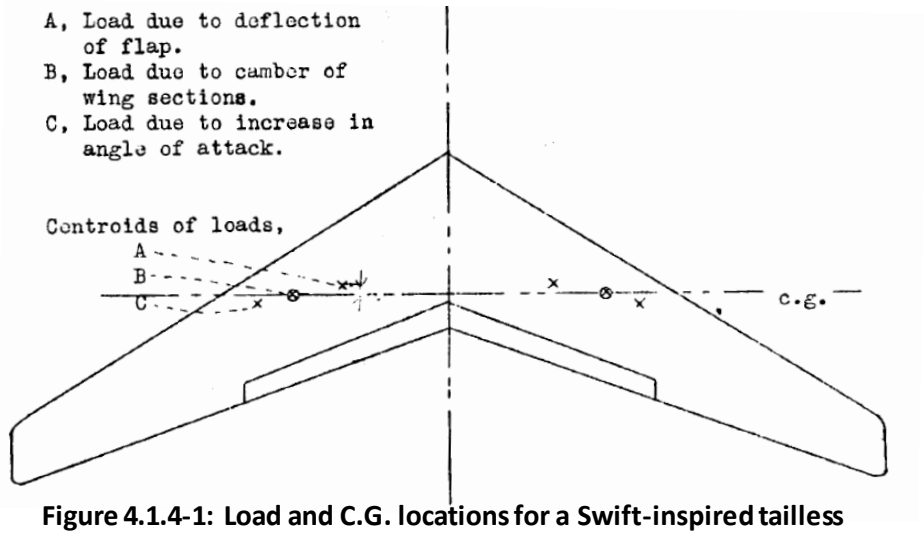

Figure 4.1.4-1: Load and C.G. locations for a Swift-inspired tailless concept [6]

4.2 Preliminary Architecture Assessment

With the preliminary architectures defined, each was analyzed to sufficiently determine its viability. As analysis progressed, concepts were eliminated until only a final design remained. This winning concept was then more closely analyzed and optimized for the design mission. The first step in the down selection process was a qualitative assessment of each architecture, shown in Table 4.2-1.

Table 4.2-1: Preliminary qualitative architecture assessment

Architecture	Pros	Cons
Twin-Boom Tail (TBT)	• Proven architecture • Structural stability	• Largest wetted area • Additional tail boom weight • Requires either long boom or large tail surfaces

Single-Boom Tail (SBT)	• Less wetted area than TBT • Conventional design path and analysis	• High structural requirements for boom • Larger wetted area than tailless concepts • Additional tail boom weight compared to tailless
Conventional Tailless (CT)	• Lower wetted area than TBT or SBT • Eliminates tail boom and tail surface weight	• Low C_{Lmax} due to lack of effective high lift devices • Larger wing area than TBT or SBT • Potential stability issues • More complex control system • Reflex camber required
Swift-Inspired Tailless (SIT)	• Lower wetted area than TBT or SBT • Eliminates tail boom and tail surface weight • Conventional airfoil sections allowable • High lift devices allowable • Smaller wing area than CT	• Potential stability issues • More complex control system • Larger wing area than TBT or SBT

4.3 Constraint Analysis

Following the methods of Brandt et al. in [7], a constraint diagram was constructed for each architecture for preliminary sizing purposes. Each of the main performance requirements from Table 1.3-1 is represented on the diagram, other than range. The TBT and SBT concepts are presented in a single diagram since there is no significant difference to the inputs. The maximum C_L required was chose such that it would not be the limiting factor of the constraint diagram, in this case 2.4. As shown in figure 4.3-1, cruise ceiling and rate of climb form the lower boundary. Since the slope of both of these boundaries are shallow in the region of the design space, a definite design point was not immediately chosen. Since the engine type is specified in the RPF, a design point would not be chosen until after a preliminary weight

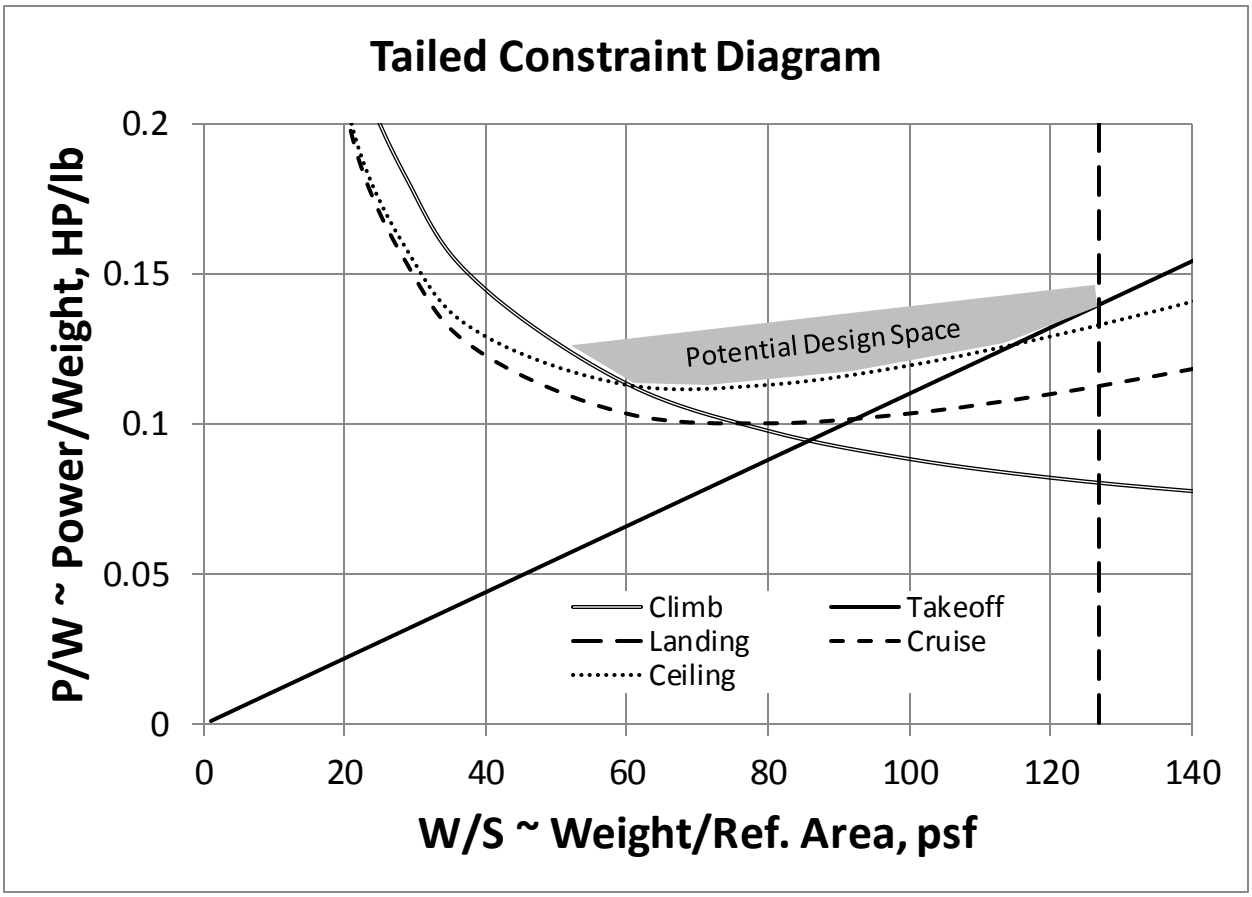

Figure 4.3-1: Tailed constraint diagram

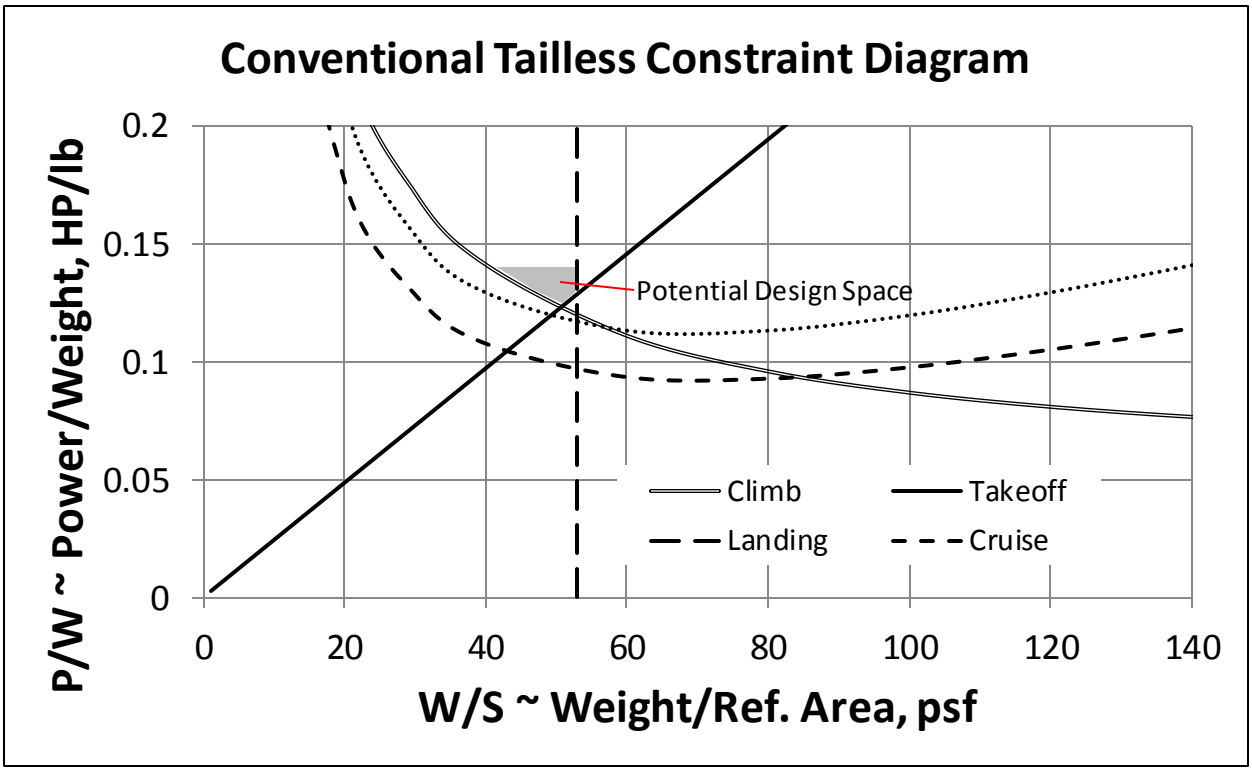

estimate, at which time the power to weight ratio of a set number of engines could be

Figure 4.3-2: CT constraint diagram

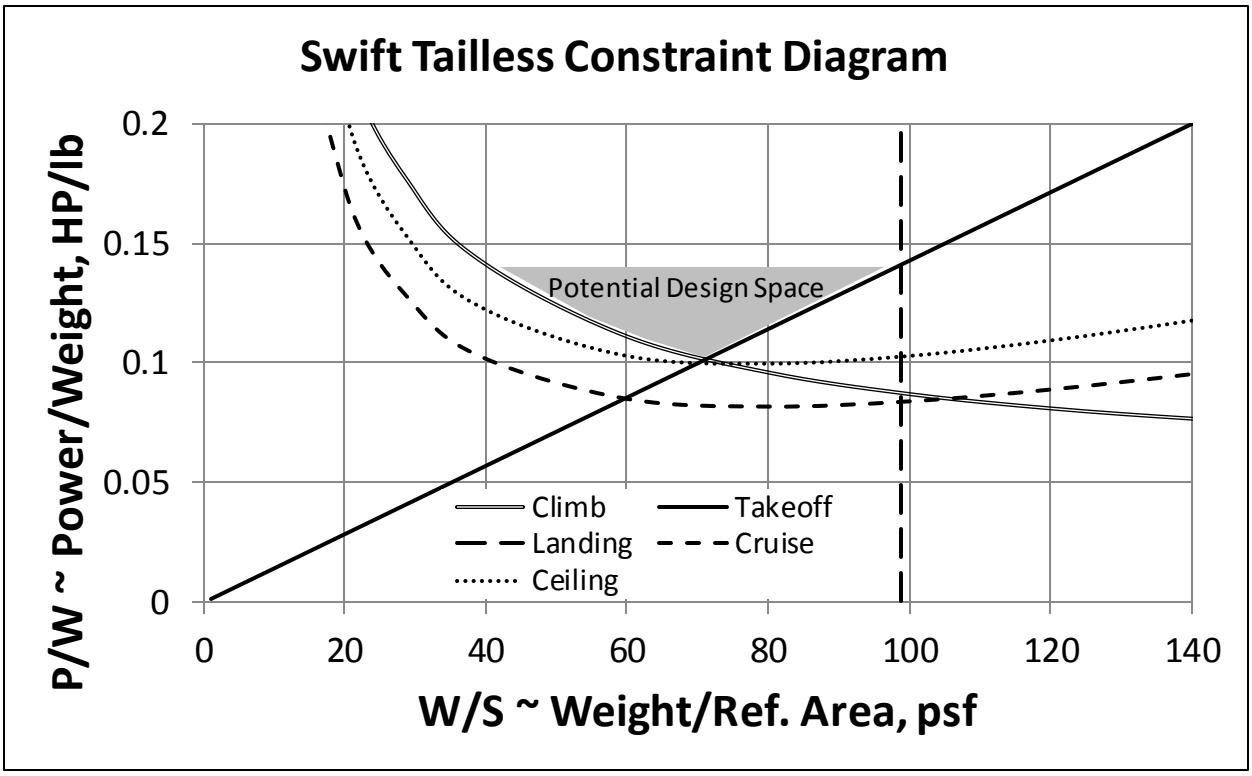

Figure 4.3-3: SIT constraint diagram

determined, then the appropriate wing loading selected from the diagram. In effect, the power loading value is quantized with only whole number multiples of the T-56 available.

For the tailless designs, the maximum C_L values were estimated from known aircraft of similar configuration at 1.0 for CT and 1.7 for the SIT. The corresponding constraint diagrams are shown in Figure 4.3-2 and 4.3-3. Though both of these constraint diagrams produced a noticeable trough to place the design point, the final design point would again be limited by the engine choice and was not immediately selected. The low lift coefficient of the traditional tailless concept is particularly problematic for takeoff and landing, a demonstration that this concept is not suitable for the short takeoff and landing (STOL) requirements of the RFP.

4.4 Preliminary Weight Estimation

A preliminary weight estimate was necessary due to the engine choice restriction provided by the RPF. From the preliminary weight estimate, the number of engines could be selected based on the constraint diagrams. Following the methods of Nicolai and Charichner [8], the weight fraction of each mission segment was calculated, as shown in Table 4.4-1. Climb and cruise were based on the minimum RFP requirements, 250 kts at 23,000 ft. A 30 minute loiter was added to the end of the mission as well as an additional 5% to the total fuel as specified in MIL-C-005011B for cargo aircraft. From the final fuel fraction and the required payload, an estimated takeoff weight of 126,000 lb was calculated. This method is independent of configuration and was assumed to be an overestimation for all configurations. All configurations have a relatively short fuselage with minimal heavy structural elements, and the tailless designs are also lacking the tail surfaces and any supporting structure. Thus, this value was used as an upper bound for the weight, and thus the power required for the configurations. Using the value of 4,300 HP provided in the RFP, three or four engines would deliver a power to weight ratio of 0.102 or 0.137, respectively. At this weight, four engines would be sufficient for any configurations, and three may be sufficient at lower takeoff weights.

Table 4.4-1: Mission weight fractions

Mission Segment	Weight Fraction
Warmup/TO	0.97
Climb	0.975
Descent	1
Landing	0.995
Cruise	0.918
Loiter 30 min	0.989
Total Mission	**0.867**
Total Fuel Fraction (+5%)	**0.184**

4.5 Preliminary Down Selection

Based on the qualitative merits and the constraint diagrams, it was decided to continue with only two concepts, the SBT and SIT. The SBT would save both weight and wetted area over the TBT configuration, and the CT required both more power and a larger wing than the

SIT. For each remaining candidate, the designs were developed enough so that a final winner could be chosen and fully developed.

5.0 Fuselage and Container Loading System

In keeping with the derived requirements from §3.0 a common fuselage was designed to be used, at least preliminarily, on both configurations. With the requirement that the container must be external to the aircraft, with no load-bearing structure around it, the fuselage has minimal structural elements. The container loading system must also be integrated into the fuselage to allow for rapid unloading of the container.

5.1 Cockpit Section

The cockpit comprises the first 18 ft of the fuselage and allows seating for the crew of 3: pilot, copilot, and loadmaster as well as electrical equipment, the environmental control system, and a small lavatory. This section of the aircraft is the only one pressurized.

5.2 Container and Loading System

The aft end of the fuselage section ends abruptly to make room for the container. The middle 21 ft of the fuselage is taken up by the container and its aerodynamic fairings. Only the top section is load-bearing and also serves as the attachment for the wing. The top structural section allows room for electrical and hydraulic lines to pass through and also houses the container loading system. The container is attached to the aircraft by means of a container spreader with four top corner twistlocks. The Lloyd's Register Rules for allowable forces on an ISO container quote a maximum tensile load on one corner of a container at 25 tonnes (55,116 lb). With all four corners secure, this is well within the limits even at the maximum load factor discussed in §17.1. The spreader is lowered by a pair of jackscrews driven by battery-powered electric motors. To both load and unload containers directly from ground level while also

accommodating container movers the spreader has a total range or motion of 3 ft, with the maximum extension of 3 ft corresponding to ground level. The sides of the container are shielded from the free stream air by a fixed aerodynamic fairing, and the bottom of the container is shielded by an extendable fairing that is extended only once the container is completely loaded. While loading, this fairing is stored rolled-up in the forward fuselage section. The cross-section in this area is rounded on the top and sides, but flat on the bottom where the bottom fairing extends.

5.3 Aft Fairing

To reduce separation drag and maintain a streamlined shape, an aerodynamic fairing is fitted after of the container for the final 11 ft of the aircraft. The fairing is simply for streamlining and does not contain any systems or other weight. It is split in half vertically down the middle and opens to allow loading access to the container. For the SBT configuration, the aft fairing blends into the tail boom much like the Blackburn Beverley in Figure 4.1.2-1.

6.0 Preliminary Wing Design

The first main feature separating the two configurations is the wing. Due to the differences in the basic concepts of the designs, the wings are necessarily unique to the configurations

6.1 SBT Wing

Due to the low speed requirement of the RFP, a straight wing was chos en for the SBT. This is well supported by historical turboprop cargo aircraft including the C-130, C-27, and An-12, among others. For preliminary comparison purposes, an aspect ratio of 8

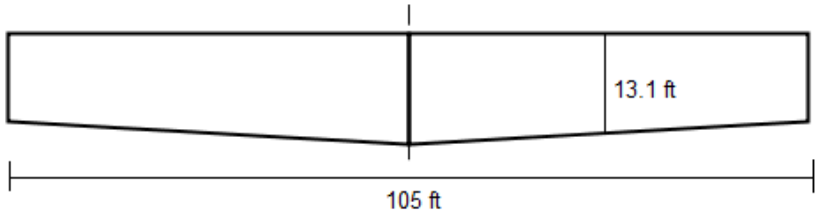

Figure 6.1-1: SBT wing planform

was chosen along with a straight leading edge and a taper ratio of 0.8. A wing loading of 90 psf is attainable with four engines and the assumed weight of 126,000 lb, which translates to a planform area of 1,370 ft^2. This planform is shown in Figure 6.1-1.

6.2 SIT Wing

Following the basic design of the Swift, The wing for the SIT configuration required moderate sweep and a relatively high taper ratio. With this in mind, a quarter-chord sweep of 20°, an aspect ratio of 10, and a taper ratio of 0.7 were chosen, emulating the Swift glider. Again assuming 4 engines, a wing loading of 90 psf was also chosen for this configuration, leading to a planform area of 1,370 ft^2, shown in Figure 6.2-1.

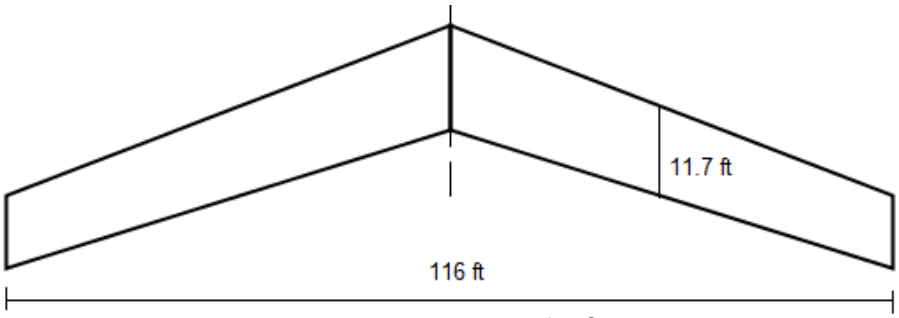

Figure 6.2-1: SIT wing planform

7.0 Preliminary Tail Design

Using historical trends, tail volume coefficients were selected for each architecture to generate an initial tail size.

7.1 SBT Tail

To minimize bending and twisting loads on the boom, a conventional tail configuration deemed most suitable for the SBT. Estimating a total arm length of 40 ft, vertical and horizontal tail volume coefficients of 0.055 and 1.0 were selected, respectively. These values correspond to tail surface areas of 197 ft^2 for the vertical

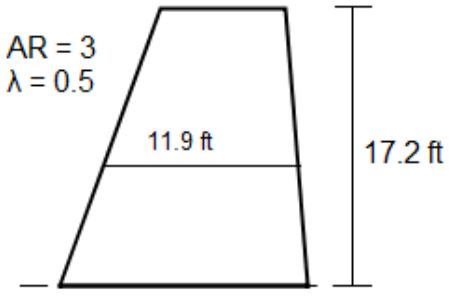

Figure 7.1-1: SBT vertical tail

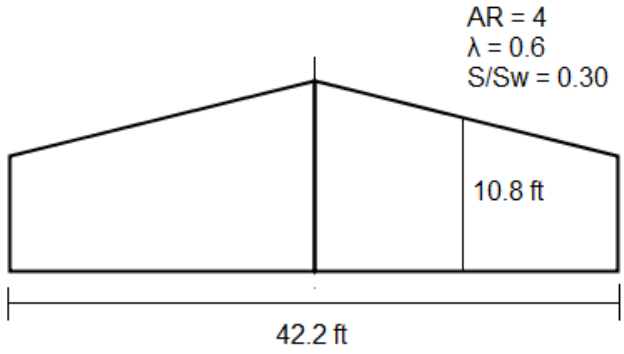

Figure 7.1-2: SBT horizontal tail

tail and 409 ft^2 for the horizontal tail. The planforms and other pertinent data are shown in Figures 7.1-1 and 7.1-2. The geometric properties were selected based on typical tail shapes of historical aircraft.

7.2 SIT Tail

Following the design of the Swift, one of the defining features of the SIT configuration is its lack of horizontal tail surfaces. It does, however, still utilize vertical tail surfaces at the wing tips. Using the wing geometry of §6.2, the moment arm is approximately 27 ft. Using a vertical tail volume coefficient of 0.06, this resulted in an area of 348.5 ft^2. Thus, each vertical tail, essentially a large winglet, has an area of 174.3 ft^2. With the root chord of this tail matching the tip chord of the wing, and a matching quarter chord sweep of 20°, the vertical surfaces appear as shown in Figure 7.2-1.

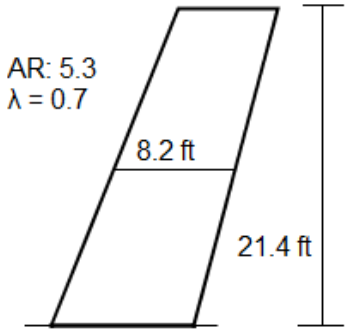

Figure 7.2-1: SIT vertical tail (one side)

8.0 Preliminary Weight Breakdown

With the basic geometries of the aircraft defined, a preliminary group weight breakdown based on the methods of Nicolai and Carichner [8] was performed. Takeoff weight is one of the most important driving factors of an aircraft, as both manufacturing and operating costs increase with increased weight. The preliminary weights of both aircraft are summarized in in Table 8.0-

Table 8.0-1: Preliminary weight breakdown

	SBT	SIT
Empty Weight (lb)	46,200	37,600
Fuel Weight (lb)	26,700	24,100
Payload (lb)	45,140	45,140
Total (lb)	118,040	106,840

1. As expected, the SBT configuration is heavier than the SIT configuration mainly due to the increased tail surface weights and the corresponding additional fuel load required.

9.0 Preliminary Cost Estimation

Based on the preliminary weights, a cost analysis was performed both for acquisition costs, using the methods of Nicolai and Carichner [8] and direct operating costs, using the methods of Sforza [10]. Both analyses assumed 2030 dollars assuming a 3.1% inflation factor, one developmental frame, and 150 production frames. The price per gallon of JP-8 was simply inflated to 2030 dollars using the current 2016 price of $5.20 per gallon. This may not accurately reflect future fuel prices, but fuel prices tend to be too variable to estimate any other way. A 1,000 nm mission as required in the RFP was assumed. As a military aircraft, no insurance or depreciation costs were accounted for. Table 9.0-1 and 9.0-2 display the acquisition and operating costs of the program, respectively.

Table 9.0-1: Preliminary development and production costs

Cost	SBT	SIT
Development	$1.1B	$930M
Total Production	$7.5B	$6.7B
Flyaway	$51M	$45M
Unit Break-Even	$58M	$51M

Table 9.0-2: Preliminary direct operating costs per mission

Cost	SBT	SIT
Fuel	$31,500	$28,400
Crew	$4,700	$4,700
Maintenance	$15,000	$13,000
Total	$51,200	$46,100

10.0 Final Configuration Down Select

Based largely on the increased weights and costs associated with the SBT configuration, the SIT configuration was selected as the final configuration to proceed with. This final configuration was given the designation “Boomerang” both due to its mission requirements and physical appearance. The concept of operations emphasizes a rapid unload of payload at its destination, meaning aircraft leaves and returns relatively quickly, and its swept, only slightly tapered wing physically resemble a boomerang.

11.0 Wing

The key to the Boomerang configuration is the properly designed wing that allows for stability while using traditional cambered airfoil sections. Thus, the initial design effort was to produce a wing suitable for the configuration.

11.1 Airfoil Selection

With a low speed requirement, a thicker airfoil section becomes advantageous both for increased structural capability leading to lower weight, and increased fuel volume capacity without critical Mach number issues. Though traditional cambered sections with negative pitching moments are usable, it is still desirable to have a relatively small negative moment, approximately. Maximum C_l is also a figure a merit in airfoil selection, as a higher attainable C_l reduces the additional C_L required from the high lift devices. NACA 6-series airfoils were the main ones considered as they are both widely used and well-documented. Table 11.1-1 summarizes the airfoils under consideration. All data displayed in this table is at a Reynold's number of 1,000,000. Though this is lower than the flight Reynold's number, this is the highest Reynold's number displayed in [12]. By comparison, the Swift's airfoil produces a pitching moment of -0.032 at an angle of attack of -0.5°.

Table 11.1-1: NACA airfoil comparison

	63-215	**63_3-218**	**63-415**	**63_3-618**	**64_3-618**	**65_2-415**
C_{lmax}	1.37	1.33	1.47	1.55	1.50	1.36
$C_{m,\alpha=0}$	-0.0396	-0.0345	-0.0790	-0.1145	-0.1146	-0.0805

Comparing the values from Table 11.1-1, both the NACA 63-215 and 63_3-218 produce acceptable pitching moments. Though the other airfoils have higher values for C_{Lmax}, their pitching moments are too negative for the configuration. In order to reduce section thickness from root to tip, the 63_3-218 was chosen for the root and the 63-215 for the tip.

11.2 High Lift Device

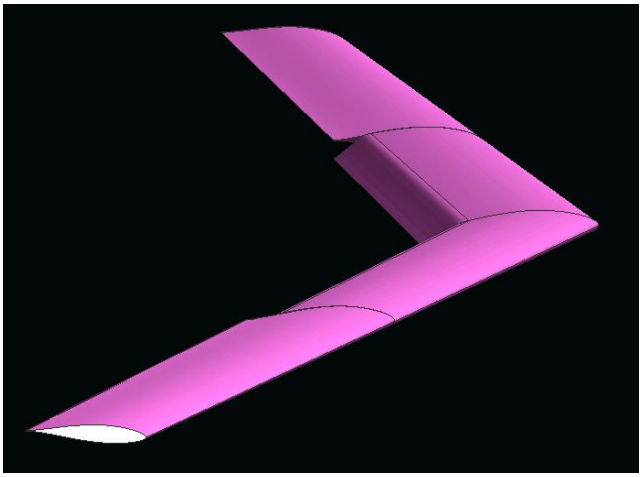

Figure 11.2-1: XFLR5 model with flap deflected

The main element that makes this configuration possible is the inboard flap that induces a lifting force far enough forward to be ahead of the CG, inducing a positive pitching moment. Like a traditional tailless configuration, however, the high lift device cannot be too effective or else the aircraft will not be trimmable at usable angle of attack. For this purpose, a 25% chord plain flap was utilized on the inboard 45% of the span that can be deflected up to 50°. An elevon will be placed outboard of the flap to the 90% span point. Following the weight and CG analysis in §18.0, XFLR5 analysis (model shown in Figure 11.2-1) showed that increasing flap deflection indeed induces a nose-up pitching moment, shown in Figure 11.2-2. Further analysis and flap trimming is discussed in §19.2.

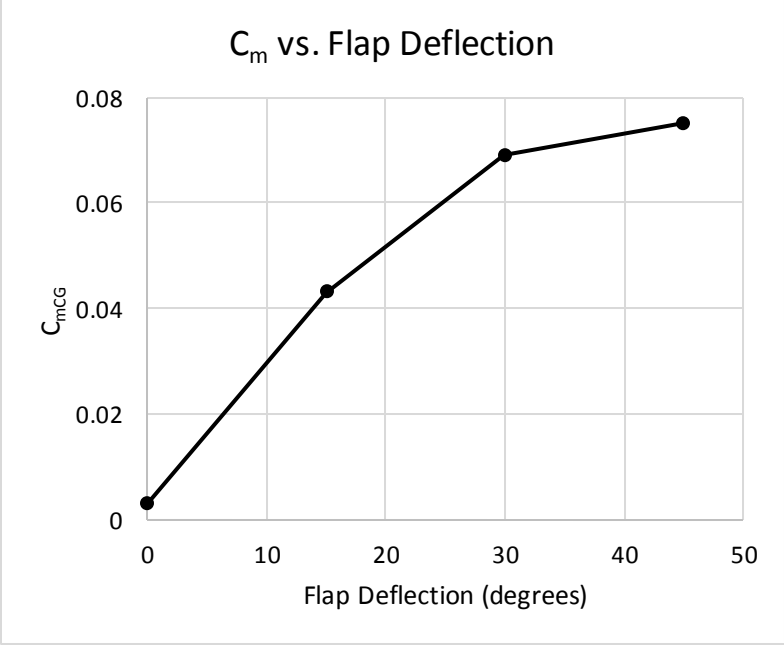

Figure 11.2-2: Cm vs. flap deflection for the most forward CG position

11.3 Planform Refinement

Though a preliminary planform was developed in §6.2, XFLR5 was utilized verify whether that planform would be suitable for the configuration. The first task was identifying the wing aerodynamic center, which for a tailless aircraft is also the neutral point. The program does not directly calculate the aerodynamic center; however, it was determined by varying the CG location and determining at what location the C_m did not change with angle of attack with no flap deflection. For this planform, the aerodynamic center was 13.15 ft aft of the root leading edge, or 23.1% of the mean aerodynamic chord, $\bar{c}$, and this point defines the extreme aft limit of the design CG since the aircraft will not be statically stable with a CG aft of the neutral point. Then, by again varying the CG location in XFLR5 while deflecting the flap at varying degrees, the point at which flap deflection did not change C_m is the center of pressure of the flap deflection alone. This point was approximately 12.3 ft aft of the root leading edge, or 15.9% $\bar{c}$, and this point defines the extreme forward design CG limit since the flap will cause a nose-down pitching moment with a more forward CG. Thus, the preliminary configuration only allows for 7.2% $\bar{c}$ CG travel, with the optimum being even less travel since there must be some margin between the points for adequate stability and trim.

In order to allow for an adequate margin between the neutral point and the flap center of pressure, the sweep was increased to 25°. Similar XFLR5 analysis placed the neutral point at 16.0 ft from the root leading edge, 23.6% $\bar{c}$, and the flap center of pressure at 14.2 ft from the root leading edge,

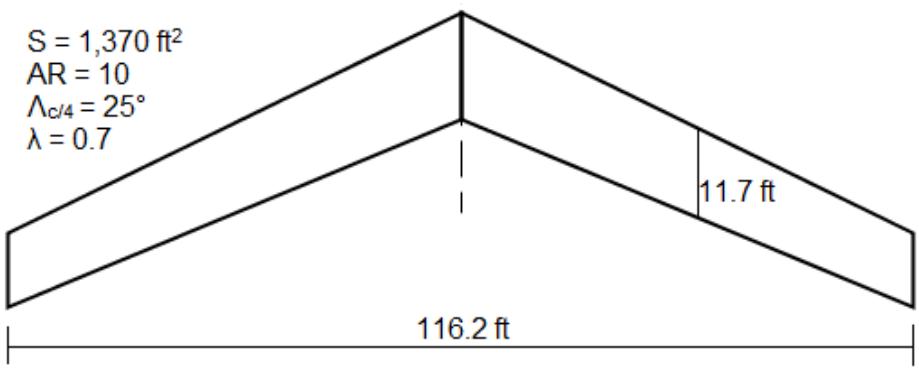

Figure 11.3-1: Refined Boomerang planform

8.25% $\bar{c}$. The increased sweep allows the maximum allowable CG travel to increase to 15.35% $\bar{c}$, allowing both a larger static margin and trim with the flap deflections. This refined planform is shown in Figure 11.3-1.

11.4 Wing Twist

As Kroo discusses in [4], a fair amount of twist is required in order to achieve an optimum elliptical lift distribution over the wing. With sweep and low taper, the wing tends to be tip-loaded, which is unsatisfactory for both induced drag and safety, as the tips would tend to stall first and greatly reduce the pilot's control of the aircraft. Using the planform defined in §11.3 with the airfoil sections discussed in §11.1, XFLR5 was used to determine the optimum amount of washout needed to obtain a roughly elliptical lift distribution. Three of these are

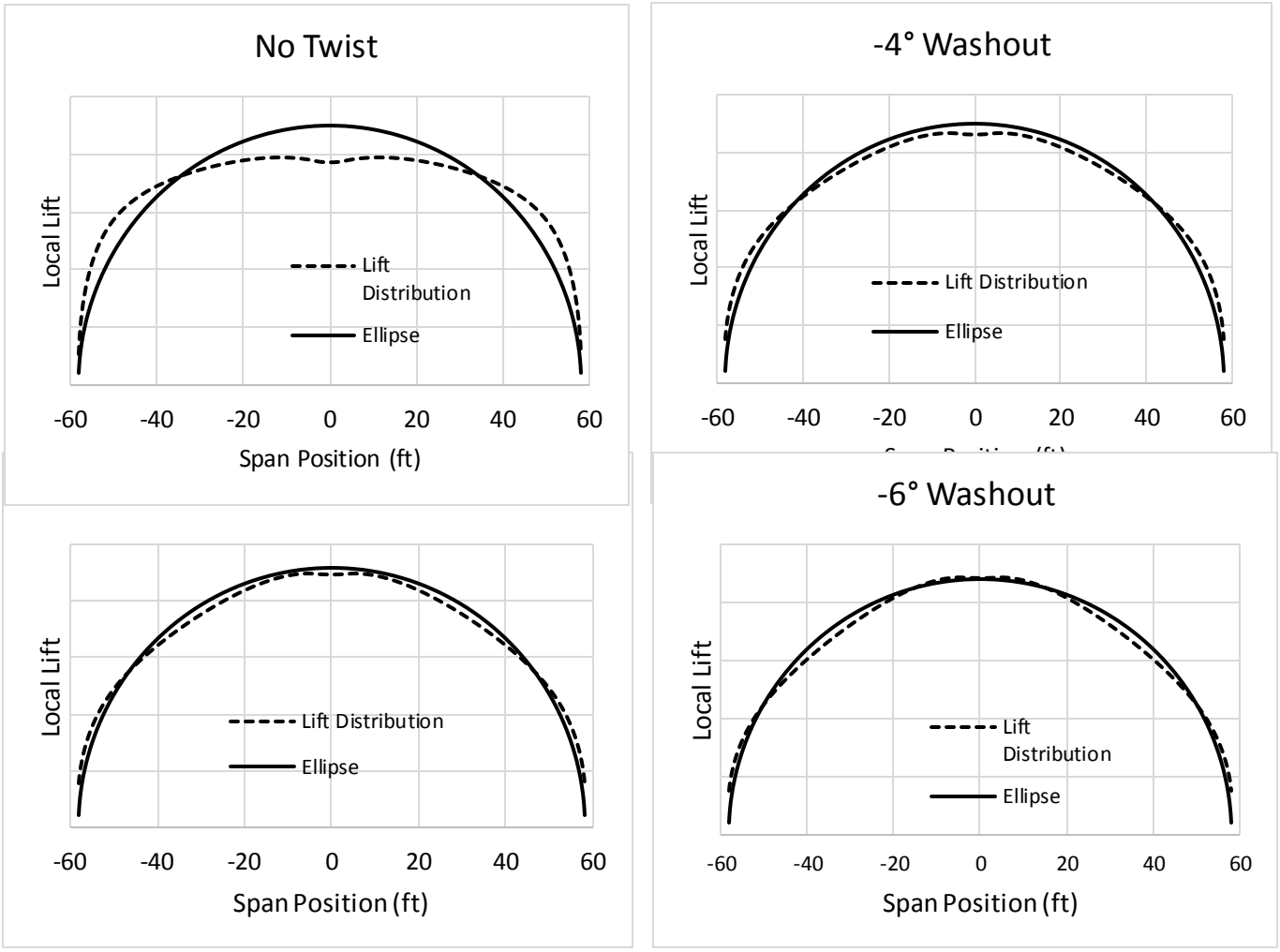

Figure 11.4-1: Lift distributions for different degrees of washout

shown in Figure 11.4-1. They cannot be all shown on the same axes because the reference ellipses are slightly different due to different lift coefficients with each twist value. From these, a washout of -5° approaches the elliptical distribution most closely.

11.5 Low Speed Lift Curves

Though XFLR5 is a powerful aerodynamic tool, it tends to overestimate stall angles of attack and the corresponding C_L values. To get a more accurate estimation of the lift curves, the methods of Nicolai and Carichner [8] were used to construct low speed lift curves with flap deflection. The characteristics near the stall angle of attack are estimated from the airfoil characteristics, which was analyzed in XFLR5 using Xfoil.

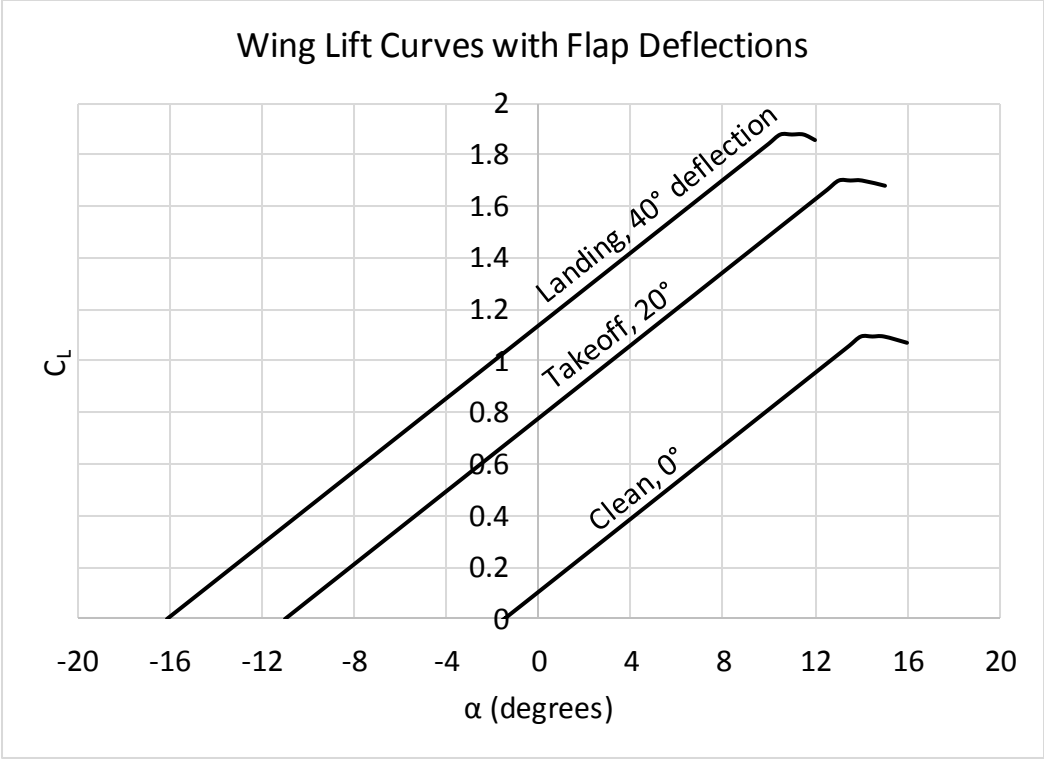

Figure 11.5-1: Lift distributions for different degrees of washout

As the figure shows, the Boomerang is able to achieve max C_L values of 1.70 for takeoff and 1.88 for landing, meeting the derived requirements of the constraint diagram. Table 11.5-1 summarizes the lifting characteristics of the aircraft.

Table 11.5-1: Lifting characteristics

Configuration	Flap Deflection (°)	α_{stall} (°)	C_{Lmax}
Clean	0	14	1.09
Takeoff	20	13	1.70
Landing	40	10.5	1.88

12.0 Propulsion System

Though the RFP specifies the powerplant choice as the Allison T-56 turboprop with NP2000 propellers this system still had to be analyzed and optimized to fit the configuration. Its available power is listed at 4,300 HP at sea level static conditions, but this engine had to be installed and analyzed at any possible conditions.

12.1 Performance Models

To analyze the engine at any potential conditions, a number of performance models were utilized, mainly from El-Sayed [12] and Anderson [13]. The main parameters of interest are the power available, thrust provided, and specific fuel consumption at real flight conditions. From the given 4,300 HP static power available, Equation 12.1-1 was used to determine power available at other conditions.

$$\frac{P_A}{P_{A0}} = \left(\frac{\rho}{\rho_0}\right)^n \qquad \text{Eq. 12.1-1}$$

Where the subscript 0 represents sea level static conditions and $n = 0.7$. With this power available, actuator disc theory was used to convert equivalent shaft power into thrust, shown in Equation 12.1-2

$$P = T(V_0 + w)$$

$$w = \frac{1}{2}\left(-V_0 + \sqrt{V_0^2 + \left(\frac{2T}{\rho A}\right)}\right) \qquad \text{Eq. 12.1-2}$$

Where V_0 is the free stream velocity, A is the propeller disc area, and w is the induced velocity. With a given power available, the corresponding thrust can be solved numerically. The engine fuel consumption was given in the RFP as 0.5 lb/hr/hp at takeoff conditions. With increasing altitude and decreasing temperature, the efficiency of the engine increases approximately as the square root of the absolute temperature ratio, as shwon in Equation 12.1-3

$$c_p = c_{p_0}\sqrt{\frac{T}{T_0}} \qquad \text{Eq. 12.1-3}$$

Where c_p is the brake specific fuel consumption, T is the absolute temerature, and the subscript 0 indicates takeoff conditions.

12.2 Number and Location of Engines

Though the RFP states the required type of engine, it does not specify the number. From the constraint diagram in §4.3, the minimum power loading required is just over 0.1 HP/lb. Though a four-engine configuration was first considered in the preliminary design, the more detailed weight of 106,840 lb would yield a power required of about 10,700 HP. Thus, only 2.5 times the power of one T-56 engine is required, making four engines significantly more power than required. After the final weight breakdown in §18.1, this power requirement decreased even further as the takeoff weight of the aircraft decreased to 92,000 lb. Though the three-engine configuration would provide weight and cost benefits, it presents the challenge of locating the middle engine along the fuselage centerline. Thus, both three and four-engine configurations were studied.

12.2.1 Tractor vs. Pusher

The majority of tailless propeller-driven aircraft including the large Northrop bombers have utilized pusher configurations for balance and CG reasons. However, the majority of aircraft favor a tractor configuration. For wing-mounted engines, both tractor and pusher

configurations are viable. A number of historical turboprop aircraft have opted for the pusher configuration including the Beech Starship 2000, Piaggio P.180 Avanti, and the AASI Jetcruzer 500. All of the aforementioned aircraft and several others in the pusher configuration use the Pratt & Whitney PT6 turboprop engine. As explained in *Flight International* [14], the PT6 is particularly suitable for a pusher configuration since it utilizes a rather unusual radial air inlet with a centrifugal compressor. Thus, it can be nearly as easily integrated as a tractor or pusher simply by rotating the exhaust stacks by 180°, as shown in Figure 12.2.1-1.

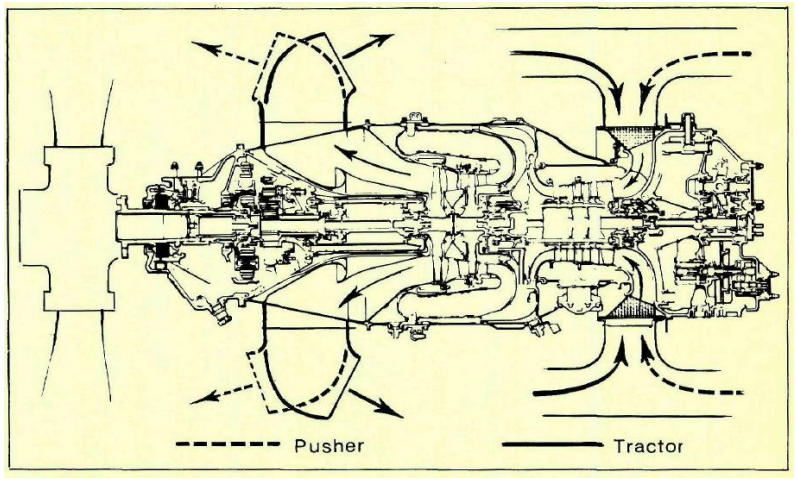

Figure 12.2.1-1: P&W PT6 inlet and exhaust schemes [14]

The Garrett TPE331 is another turboprop that has been used in a pusher configuration on several aircraft including the General Atomics MQ-9 Reaper and the Cessna Skymaster O-2. Though it uses a centrifugal compressor, it displays more traditional forward-facing inlet and rear-facing exhaust, shown in Figure 12.2.1-2. The T-56 utilizes the same "straight through" inlet and exhaust, though with an axial flow compressor. Thus, while a pusher configuration is not impossible, significant ducting would be required to turn the flow 180° into the inlet and again turn it 180°

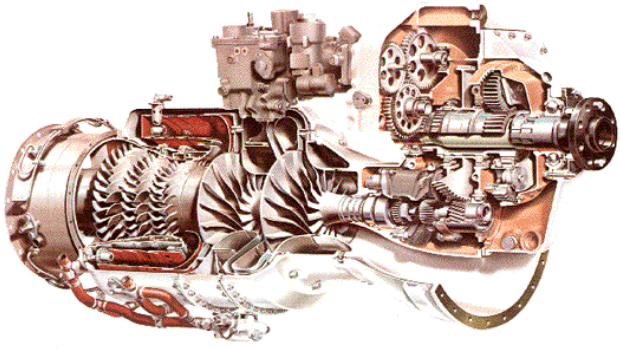

Figure 12.2.1-2: Garrett TPE331 internal arrangement[6]

[6] http://www.aircraftenginedesign.com/pictures/TPE331.gif

after the exhaust. The pusher configuration also has the drawback of reducing the amount of trailing edge width available for the control surfaces. With this in mind, it was decided to focus primarily on tractor engine configurations and only resort to a pusher if no other solution was available.

12.2.2 Four-Engine Configuration

Aircraft with four wing-mounted turboprops are numerous, including the de Havilland Canada DHC-7 and Lockheed C-130, indicating a robust configuration. Though the tailless configuration does face some CG difficulties, a properly configured aircraft can maintain acceptable CG travel. For the Boomerang, four engines are acceptable, though it would be over 60% overpowered. The main advantage of the four-engine configuration is its inherent symmetry without locating one engine on the fuselage centerline.

12.2.3 Three-Engine Configuration

Owing to the excess power and weight of a four-engine configuration, a three-engine configuration was also studied. Simply removing one engine immediately saves approximately 6,000 lb, without regard for other areas of the aircraft that would be impacted. The unit break even cost is also impacted, increasing roughly $5 million. For example, the elimination of the outboard pair of engines would also reduce the tail size needed to maintain a straight course in the case of an engine failure on takeoff. The main difficulty of the configuration is the location of the center engine. Most jets as well as the propeller-

Figure 12.2.3-1: The unique Conroy Tri-Turbo-Three[7]

[7] http://www.airport-data.com/images/aircraft/small/000/381/381556.jpg

driven Britten-Norman Trislander solved this by locating the third engine in the tail, an option not available to the Boomerang.

The only other option was to locate the engine at the aircraft's nose. This configuration has been successfully used on several aircraft including the Ford Trimotor, Junkers Ju 52, and the Conroy Tri-Turbo-Three modified turboprop DC-3 shown in Figure 12.2.3-1. Though this is the only practical installation of a center engine in the boomerang, it is not without difficulties. Due to the large propeller diameter, ground clearance must be addressed, and the engine must be properly exhausted from its position in the nose of the aircraft. Following the landing gear design in §22.0, for adequate propeller clearance, the engine needs to be located 3.5 ft above the fuselage floor line. Despite the difficulties in installation, the weight savings of more than 6.5% and unit cost savings of approximately 9% are significant enough to choose the three-engine configuration over the four-engine.

12.3 Engine Orientation

The Allison T-56 can be installed either gearbox-high, as with the C-130, or gearbox-low, as with the P-3. All three engines will be installed gearbox-high. The nose engine benefits from raising the propeller to increase ground clearance, and the wing-mounted engines will allow more room for the landing gear to retract into.

13.0 Vertical Tail and Rudder Sizing

The two criteria sizing the vertical tail fins are the maintenance of directional control in case of an asymmetrical engine-out scenario and strong crosswind landing. Both analyses were performed concurrently until a configuration was reached that satisfied both requirements.

13.1 Engine-out Takeoff

The one engine out analysis assumed that the inoperative engine is unable to feather the propeller and thus causes drag on that side. At the outset of the one engine out analysis, it was determined that the original tail fins of Figure 7.2-1 were far larger than required for adequate control. A maximum rudder deflection of 20° as suggested in [8] was also used. Stability and control derivatives were calculated using the methods of Roskam [15]. After iterating several vertical tail and rudder configurations along with the crosswind requirements of §13.2, the final configuration is as shown in Figure 13.1-1. The rudder spans 80% of the vertical fin and comprises 30% of its total area. Figure 13.1-2 also shows the derivation of the minimum control speed of the Boomerang of 124 kt, 5 kt slower than the minimum takeoff speed of 129 kt.

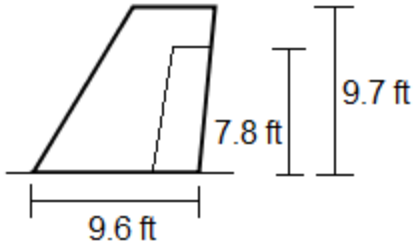

Figure 13.1-1: One side vertical tail fin

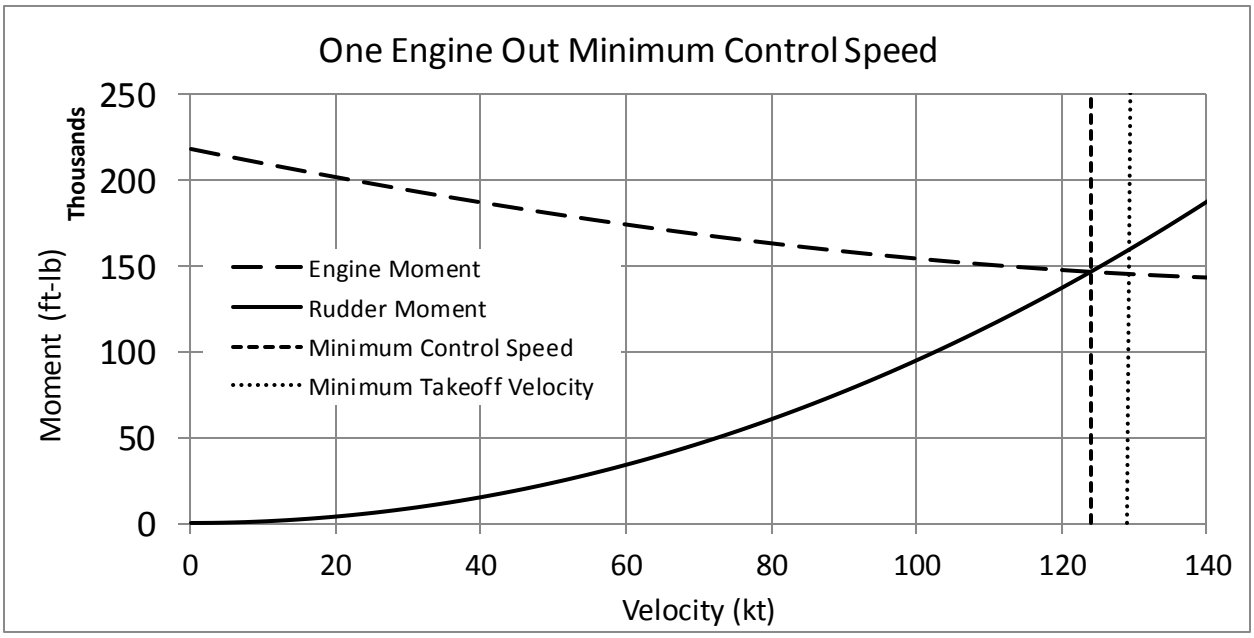

Figure 13.1-2: Minimum Control Speed with One Engine

13.2 Crosswind Landing

Though Nicolai and Charichner recommend a crosswind speed of 20% minimum speed (110% stall speed), this was only 21 kt for the Boomerang. All comparable large aircraft listed in Sadraey [16] are able to land with at least a 30 kt crosswind; thus, this value was chosen as the requirement. Using stability derivatives calculated from Roskam, Sadraey presents two equations, presented here as Equations 13.2-1 and 13.2-2, to solve simultaneously to determine δ_R, the rudder deflection, and σ, the crab angle on approach.

$$\frac{1}{2}\rho V_T^2 Sb\left(C_{n_0} + C_{n_\beta}(\beta - \sigma) + C_{n_{\delta_R}}\delta_R\right) + F_w d_c \cos\sigma = 0 \qquad \text{Eq. 13.2-1}$$

$$\frac{1}{2}\rho V_w^2 S_S C_{D_y} - \frac{1}{2}\rho V_T^2 S\left(C_{y_0} + C_{y_\beta}(\beta - \sigma) + C_{y_{\delta_R}}\delta_R\right) = 0 \qquad \text{Eq. 13.2-2}$$

Where Table 13.2-1 lists the variables other than the ones typically encountered.

Table 13.2-1: Variables in Eq. 13.2-1 and 13.2-1

C_{D_y}	Side drag coefficient
d_c	Distance between projected side area center and CG
F_w	Crosswind force on side of aircraft
S_S	Projected side area
V_T	Total velocity
V_w	Crosswind velocity

Solving these two equations numerically, after several vertical tail and rudder configurations, yielded final values of 19.7° rudder deflection required for a 25.8° crab angle for the crosswind landing. With both the one engine out takeoff and crosswind landing requirements satisfied, the vertical tail fins are acceptable.

14.0 Drag Buildup

A two term drag polar was used for all flight conditions. Since the speed requirements are quite low, the critical Mach number would not be reached, so wave drag was not considered. A

separate drag polar for each altitude and speed was constructed to take into account Reynold's number effects.

Table 14.1-1: Zero lift drag models

Component	K	C_F	S_{wet}
Wing and Tail	$2.7\left(\frac{t}{c}\right)_{max} + 100\left(\frac{t}{c}\right)^4_{max}$	$(1 - 0.072M^{1.5})\frac{0.0315}{Re_{MAC}^{\frac{1}{7}}}$	$S\left[2\left(1+\left(\frac{t}{c}\right)_{max}\right)\left(1-\eta_b\frac{2-(1-\lambda)\eta_b}{1+\lambda}\right)\right]$
Fuselage	$1+\frac{60}{F^3}+0.0025F$	$(1 - 0.072M^{1.5})\frac{0.0315}{Re_{Fus}^{\frac{1}{7}}}$	$4A_0\left(F-\frac{F_{NC}}{3}-\frac{F_{TC}}{2}\right)$
Nacelle	Same as above	Same as above	Same as above

14.1 Zero Lift Drag

The methods of Sforza [10] were used to estimate the parasite drag component by component using Equation 14.1-1.

$$C_{D_0} = \sum_{i=1}^{n} K_i C_{F_{turb_i}} \frac{S_{wet_i}}{S} \qquad \text{Eq. 14.1-1}$$

Where the subscript *i* identifies each different aircraft component, *K* is a form factor correction, C_F is the average turbulent skin friction coefficient of a flat plate of length equal to the mean aerodynamic chord of the wing, and S_{wet} is the wetted area of the component. Table 14.1-1 summarizes the relations used for each aircraft component to determine the drag.

Where, other than the commonly encountered variables, η_b is the proportion of the semi-span of the wing that is covered by the fuselage, F is the fineness ratio, A_0 is the fuselage cross-sectional area, and the subscripts *NC* and *TC* correspond to nosecone and tailcone, respectively. In the takeoff and landing configurations, landing gear and flap increments to zero lift drag are also taken into account directly using Equations 14.1-2 and 14.1-3, respectively.

$$C_{D_{0,LG}} = 1.79 \times 10^{-3} \frac{W_{TO}^{.785}}{S} \qquad \text{Eq. 14.1-2}$$

$$C_{D_{0,flap}} = 0.9\left(\frac{c_{flap}}{c}\right)^{1.38}\left(\frac{S_{w_{flap}}}{S}\right)\sin^2\left(\delta_{flap}\right) \qquad \text{Eq. 14.1-3}$$

Where $S_{w,flap}/S$ is shown in Figure 14.1-1.

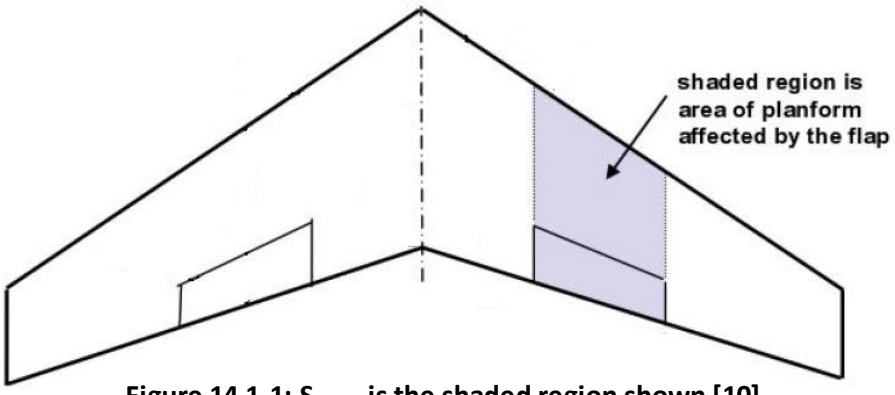

Figure 14.1-1: $S_{w,flap}$ is the shaded region shown [10]

An additional 5% miscelaneous drag was also added as recommended in [10]. Though a unique zero lift drag was found for every flight condition, Table 14.1-2 shows a representative drag buildup for the takeoff configuration.

Table 14.1-2: Takeoff 20° flap deflection drag buildup

Component	Reference Length (ft)	S_{wet} (ft^2)	Re (10^6)	F or t/c	K	C_F	ΔC_{D0}
Wing	11.7	2900	13.4	0.18	1.60	0.0030	0.0103
Flaps							0.0070
H Tail							
V Tail (x2)	7.44	153	8.51	0.10	1.28	0.0032	0.0005
Fuse	50	1552	57.2	4.2	1.84	0.0024	0.0052
Nacelle (x2)	12.2	191	13.9	2.4	1.78	0.0030	0.0008
Landing Gear							0.0125
Sum							0.0373
Misc (5%)							0.0019
Total							**0.0392**

14.2 Drag Due to Lift

The induced drag term shown in Equation 14.2-1 is then added to the zero lift drag to create the final drag polar.

$$C_{D_i} = \frac{C_L^2}{\pi e AR} \qquad \text{Eq. 14.2-1}$$

The only unknown parameter here is *e*, the Oswald efficiency factor. A paper written by Nita and Scholz [17] outlines a method for determining the Oswald factor by determining a maximum theoretical value based on the aircraft's geometry and then applying a number of correction factors that take into account not only geometry but flight Mach number as well. Thus, the Oswald factor is a dynamic measure that changes during the flight. Winglets can also be taken into effect, which applies to the Boomerang's vertical tail fins. At subsonic flight Mach numbers, the aircraft velocity has very little impact on the Oswald factor, so for all flight conditions the factor used for the Boomerang was calculated to be 0.843. This value takes into account the effect of the winglets; without winglets the factor is 0.735.

14.3 Drag Polars

With both the zero lift and induced drag terms accounted for, a complete drag polar could be constructed, shown in Figure 14.3-1. The takeoff and landing configurations include both flap and landing gear drag, and as expected both significantly increase available lift and increase total drag. The clean configuration is taken at 23,000 ft with a velocity of 250 kts. Increasing cruise speed decreases drag slightly due to Reynold's number effects, and a unique parasite drag and thus drag polar was constructed for all cruise conditions analyzed in the following section. L/D curves were also

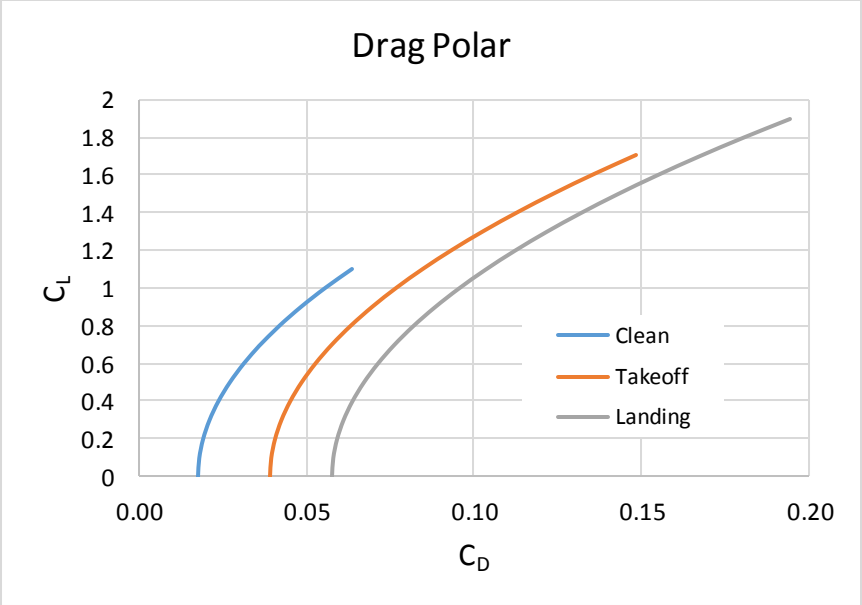

Figure 14.3-1: Drag polar for cruise, takeoff, and landing configurations

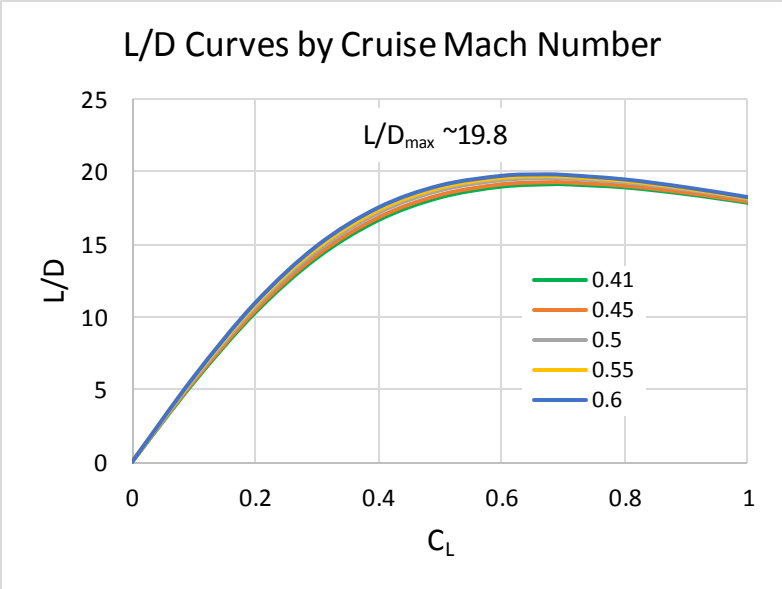

Figure 14.3-2: L/D curves for cruise

constructed at various Mach numbers, and increasing speed below the critical Mach number tended to increase L/D_{max} with the slight reduction in skin friction drag, shown in Figure 14.3-2. Though this an indication that cruising above the minimum required speed may be advantageous, it was not known exactly what would be the most efficient cruise speed and altitude. It is also worth noting that the lift coefficient for max L/D occurs around 0.67.

15.0 Climb, Ceiling, and Operational Envelope

15.1 Climb at 10,000 ft altitude

One of the specific RFP requirements calls for a rate of climb of at least 1,500 ft/min at 10,000 ft altitude at the takeoff weight. From a given altitude, rates of climb were calculated at a range of flight speeds using Equation 15.1-1.

$$\frac{R}{C} = V\left(\frac{T}{W} - \frac{qC_{D_0}}{\frac{W}{S}} - \frac{n^2 KW}{Sq}\right) \qquad \text{Eq. 15.1-1}$$

Where other than the typical variables, n is the load factor and K is the induced drag coefficient. For 10,000 ft, Figure 15.0-1 was generated, which displays the Boomerang's max rate of climb of 2,140 ft/ min at 300 kt. However, due to Federal Aviation Regulations (FARs), aircraft are not allowed to operate at over 250 kt under 10,000 ft. Even with this restriction, the Boomerang still meets the requirement with a rate of climb of 2,030 ft/min at 250 kt.

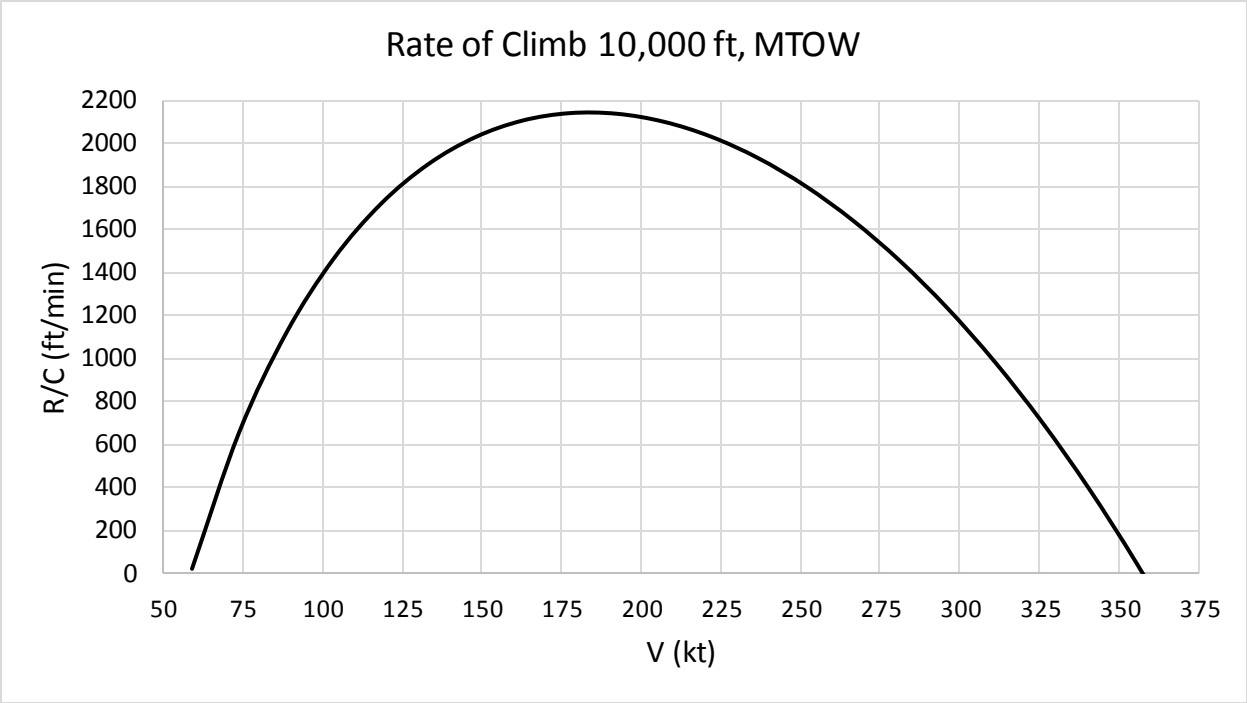

Figure 15.0-1: Rate of climb at 10,000 ft, max takeoff weight

15.2 Ceiling and Operational Envelope

The ceiling and operational envelope of the Boomerang were determined concurrently. For each altitude, the rate of climb in Equation 15.1-1 was set to 100 ft/min, and the flight speed

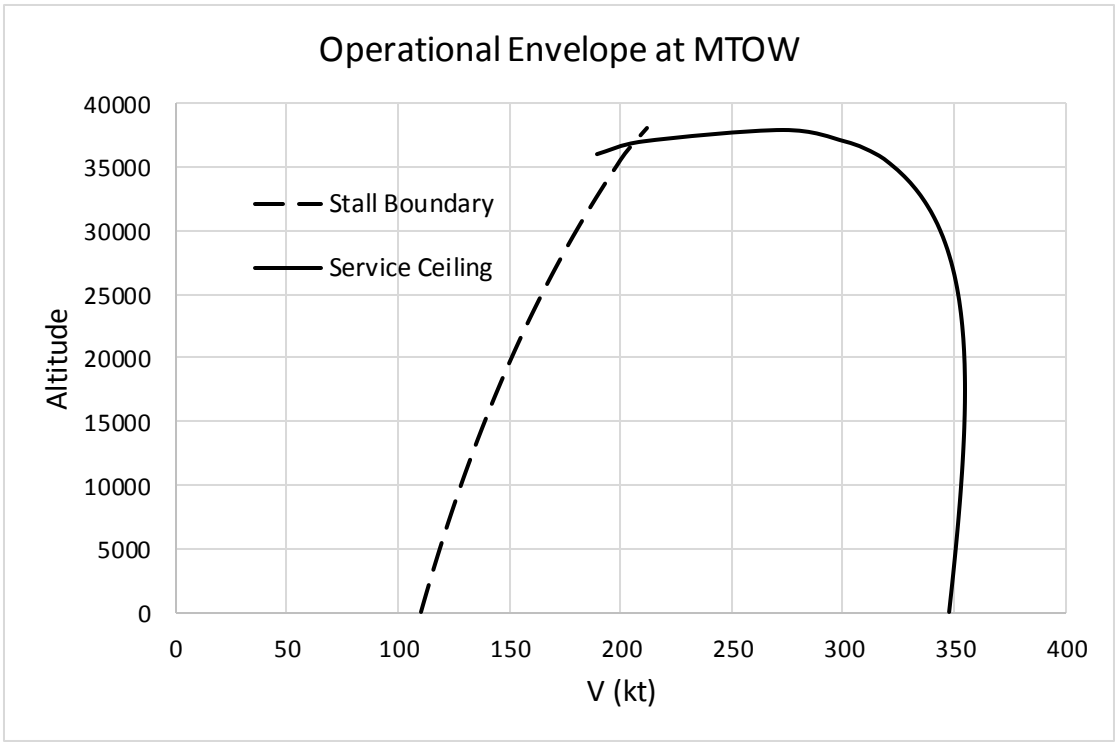

Figure 15.2-1: Max takeoff weight operational envelope

corresponding to that rate of climb was numerically determined taking into account the change in available thrust with changes in speed. This was plotted with the stall speeds in Figure 15.2-1, which increase with altitude due to the change in air density. This graph defines the Boomerang's operational envelope at all speeds and altitudes for its maximum takeoff weight.

At max takeoff weight, the max service ceiling is 37,900 feet. A similar procedure was followed for a ferry configuration without the payload, and the ceiling increased to 41,000 ft, surpassing the RFP requirement of 33,000 ft.

16.0 Optimum Cruise Performance

Though the RFP's minimum cruise requirements are 250 kts at 23,000 ft, this may not correspond to the most efficient cruise performance. To determine the best cruise conditions, Torenbeek [18] presents a very in-depth analysis. One method in particular makes use of the range parameter, *V/F*, where *V* is the cruise velocity and *F* is the fuel flow rate. Maximizing this parameter necessarily results in the most fuel efficient cruise. This method takes into account both the engine efficiency and the aerodynamic efficiency to find the overall most efficient point, which may or may not coincide with the maximum engine or aerodynamic efficiency. Repeating Equation 12.1-3, the brake specific fuel consumption decreases with decreasing temperature, and thus increasing altitude.

$$c_p = c_{p_0}\sqrt{\frac{T}{T_0}} \qquad \text{Eq. 12.1-3}$$

The aerodynamic efficiency takes into account the unique drag polars for each altitude and Mach number. For ease of analysis, curve fits were generated for the parasite drag coefficient at each altitude. Figure 15.0-1 shows an example for 23,000 and 25,000 ft, though curves were generated ever 2,000 ft between 23,000 ft and 39,000 ft.

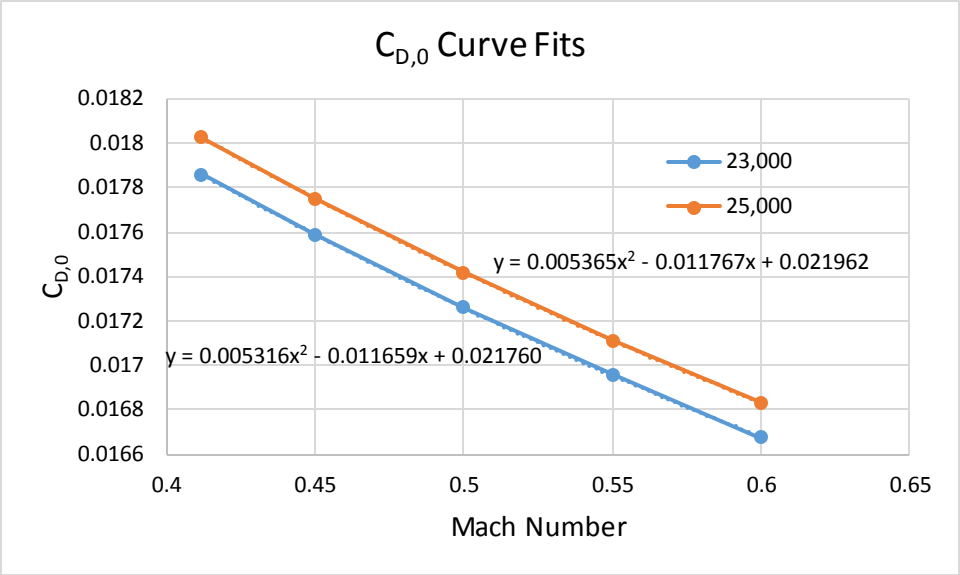

Figure 16.0-1: Drag coefficient curve fit example

To generate cruise efficiency curves, given range parameter value and altitudes were selected, and then the Mach number corresponding to those two values was numerically solved for. Points of equal range parameter were then connected to form closed contours. The 250 kt minimum cruise speed boundary and operational envelope are also superimposed in order to

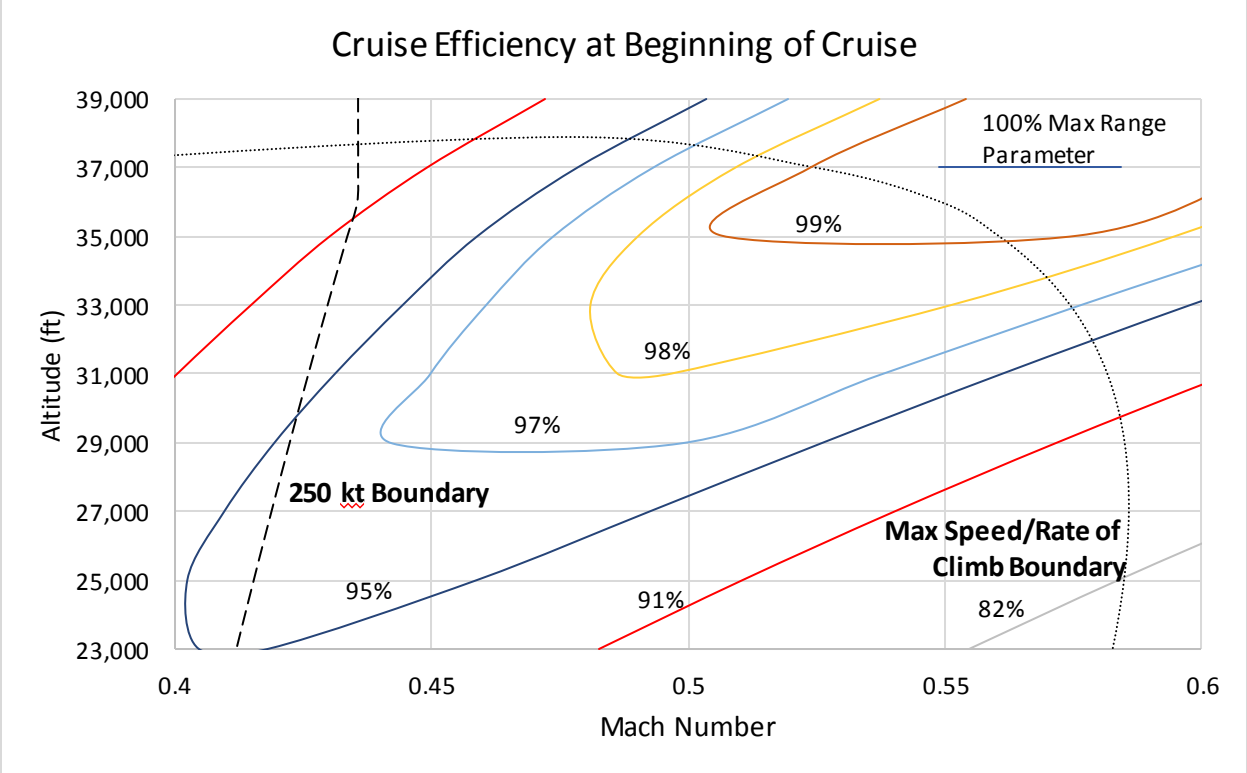

Figure 16.0-2: Cruise efficiency contours

create an allowable cruise space within the contours. This is all shown in Figure 16.0-2. Due to the tediousness of the calculations required, relatively few points were plotted, making the contours look less evenly spaced and more oddly shaped than they really should be. And as stated above, these are closed contours, though most of them close outside the chart area.

Figure 16.0-2 displays the contours for the aircraft weight at the beginning of cruise, but two additional graphs were constructed representing the weight at the middle of cruise and the end of cruise. To calculate total cruise fuel, the range parameter must be integrated over the distance of the cruise segment. Since range parameter values are only available at the beginning, middle, and end of cruise, cruise fuel weight was estimated by assuming an average value of the range parameter on a segment of the cruise length.

16.1 Optimum Mission Profile

Though the most efficient cruise is in the upper corner of the graph, at roughly 36,000 at Mach 0.55, the entire mission fuel must be taken into account, including the fuel required to climb. Though the cruise efficiency at the minimum RFP requirements of 23,000 ft at 250 kts is only several percent less efficient, the climb to the lower altitude would require less fuel. In [10] Sforza describes a method to calculate fuel burned to climb as well as the horizontal distance covered during climb. To determine the minimum mission fuel required, two different mission profiles were considered, a climb to 23,000 ft and a

Table 16.1-1: Mission fuel comparison

	Profile 1	Profile 2
Cruise Mach	0.421	0.53
Altitude 1 (ft)	23,000	36,000
Fuel to Climb (lb)	808	1,658
Horizontal Distance Climbing (nm)	47	200
Distance @ Altitude 1 (nm)	953	400
Range Parameter @ Altitude 1 (ft/s/lb)	876	908
Altitude 2		37,000
Distance @ Altitude 2 (nm)		400
Range Parameter @ Altitude 2 (ft/s/lb)		943
Total Cruise Fuel (lb)	6607	5252
Loiter Fuel (lb)	195	195
Total Fuel +5% (lb)	**7991**	**7460**

constant 250 kt cruise, and a climb to 36,000 ft and a cruise at Mach 0.53 followed by a step up to 37,000 ft halfway through the remaining cruise length. Table 16.1-1 Summarizes the results, also taking into account the fuel required for a 30 minute loiter and an additional 5% added to the total. Even though the higher, faster cruise burns more than double the fuel to climb to altitude, the horizontal distance travelled while climbing allows the total mission fuel to remain lower overall by 6.6%, a large margin when comparing fuel burn. As the final entries show, the mission fuel requirements are significantly lower than the original estimate of over 20,000 lb. Also note that the cruise lift coefficient for the high, fast cruise is approximately 0.68 for both segments, resulting in an L/D of 19.0

17.0 Structures and Materials

17.1 V-n Diagram

The V-n diagram shown in Figure 17.1-1 was constructed using the methods of Sadraey [16]. The maximum load factors given for a transport are +3 and -1. The diagram was constructed for the cruise altitude of 36,000 ft, and the corresponding gust velocities are 18.3,

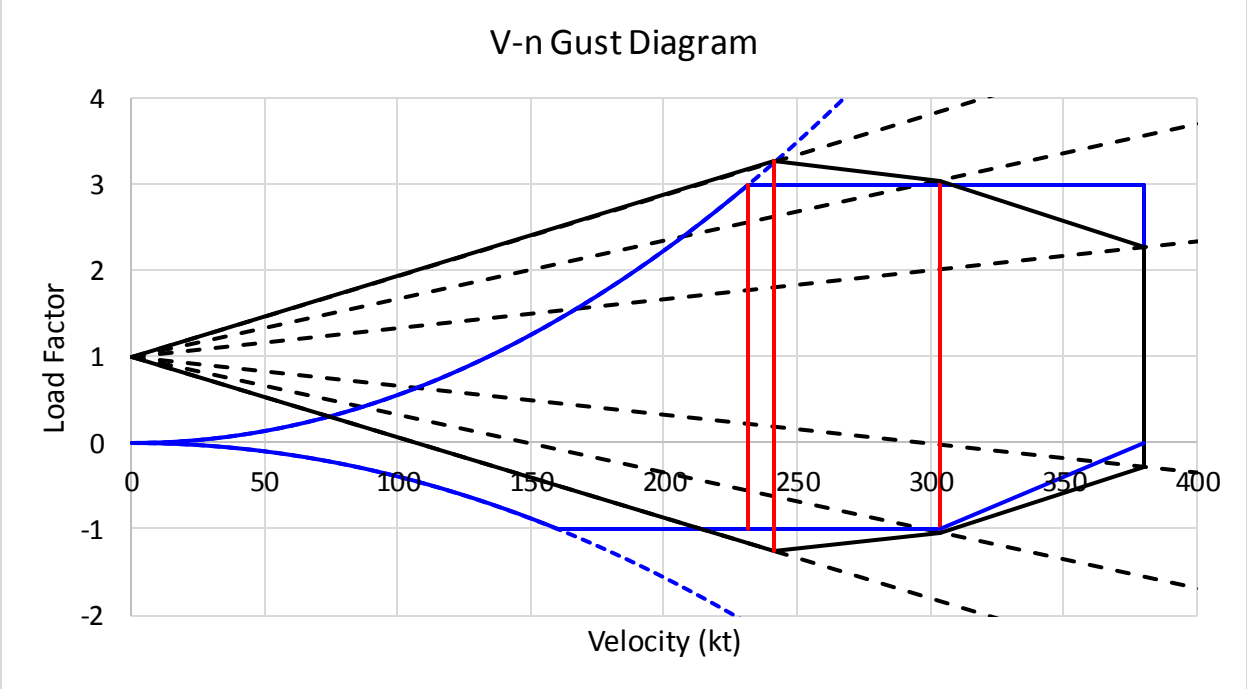

Figure 17.1-1: V-n gust diagram at 36,000 ft

36.7, and 51.0 ft/s. NACA TN837 notes, however, that tailless aircraft are naturally resistant to gust effects. Since the aerodynamic center is after of the CG, any vertical gust load will lower the nose and automatically alleviate the effects.

17.2 Wing Structure

According to Nicolai and Carichner [8], composite wing structure as opposed to traditional metallic structure can save 20% of the wing weight. The Boeing 787 wing, for example, is composed primarily from composite materials in order to capture this weight savings. With over 400 in service as of April 2016, the composite wing is shown to be a mature technology even for large, high aspect ratio wings. It was thus an easy decision to use carbon fiber-reinforced plastics (CFRP) for the Boomerang wing. The next design consideration was the wing internal arrangement, either a multi-rib wing or a multi-spar wing, as shown in Figure 17.2-1. Due to the large aspect ratio and high thickness, the multi-rib wing is the superior choice and

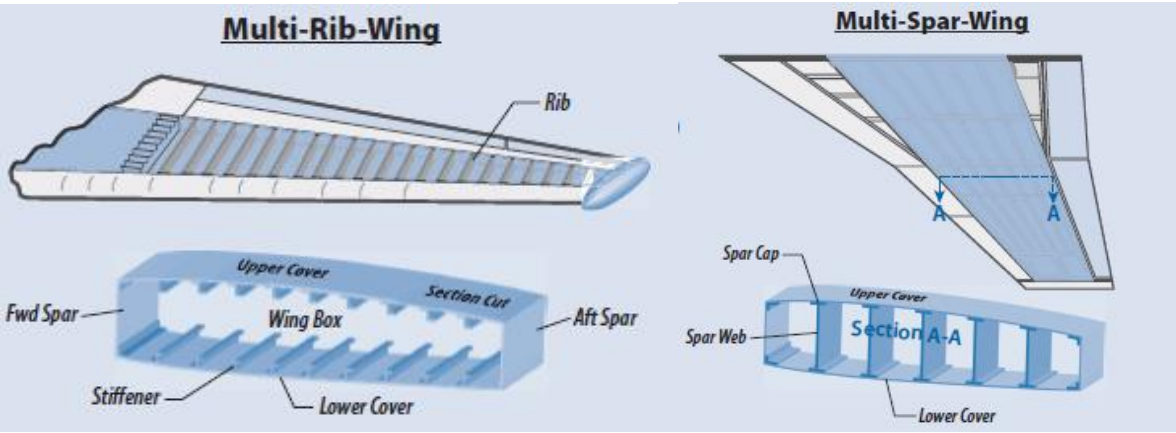

Figure 17.2-1: Multi-rib vs. multi-spar wing structures [8]

also allows sufficient room for fuel storage. The rear spar is placed at 75% chord for control surface attachment, and the forward spar is placed at 15% chord. Similarly, the vertical tail fins are also made out of CFRP for weight savings. The leading edges of the wing remain aluminum to maintain impact resistance in case of foreign object debris encountered on the runway or hail or bird strikes encountered in the air.

17.3 Fuselage Structure

The Boomerang fuselage is very non-traditional since the majority of it is not load bearing. The fuselage is essentially made up of three main sections: the forward cockpit section, the payload section, and the aft fairing.

17.3.1 Forward Fuselage

The forward fuselage contains the cockpit, small lavatory, environmental control system, and avionics required for the aircraft. It follows the skin-stringer approach of [8] shown in Figure 17.3.1-1. Since the fuselage does not make up a large portion of the overall weight, aluminum is used for the main structure both for strength and easy of manufacture and repair. The wing root leading edge is also located in the forward fuselage. The forward fuselage is connected to the mid fuselage at the upper 3 ft of the structure. Since this is an area of stress concentration, titanium strengthening is used in this area. The rearmost bottom section also houses an extendable fairing to cover the bottom of the container once in place.

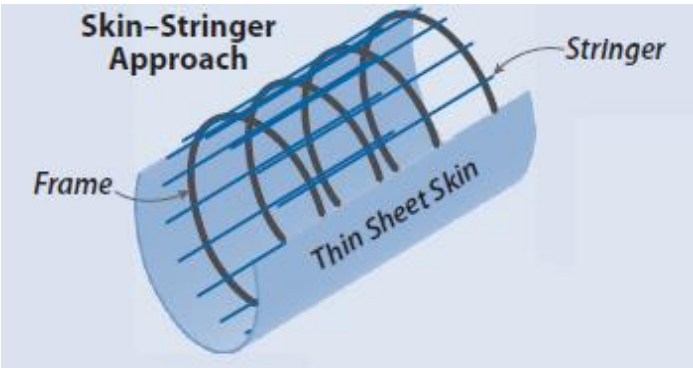

Figure 17.3.1-1: Skin-Stringer fuselage structure approach

17.3.2 Mid Fuselage

The mid fuselage serves as both the payload and wing attachment point. The main structural area is the upper 3 ft. The upper section of the mid fuselage houses the container spreader, batteries, and electric motor of the payload integration system as well as the wing carry-through. A steel frame extends down to support a CFRP aerodynamic shell around the container. The bottom of the frame is a rail that the extendable fairing slides along. The rearmost

part of the extendable fairing is a steel bar that locks into place at the end of the rail, providing some structural rigidity for the frame after the container has been loaded.

17.3.3 Aft Fuselage

The aft fuselage is completely comprised of a hollow CFRP aerodynamic fairing covering the rear of the container. It is split longitudinally down the middle and each side is linked to the mid fuselage by a rotating link at the top of the fuselage. When loading or unloading a container, the pieces swing away to allow full access to the mid fuselage.

18.0 Weight and Balance

A component weight buildup was performed to improve the accuracy of the total aircraft weight and a determination of CG travel.

18.1 Component Weight Buildup

Using the methods of Nicolai and Carichner [8] and Roskam [19], the weight of each unknown component was determined using historical trends, shown in Table 18.1-1. Many components such as the avionics and environmental control are included in the miscellaneous entry. The MTOW of 92,400 lb has been used throughout this report.

Table 18.1-1: Component weight buildup

Component	Weight (lb)
Wing	7200
Vertical Tail Fins	520
Fuselage	1850
Landing Gear	6000
Engines + Props	14500
Fuel system	1030
Misc	5550
Payload Loading System	2200
Structure Total	**39800**
Payload	45140
Fuel	7500
MTOW	**92400**

18.2 CG Travel

Though important for any aircraft, the CG travels for the Boomerang is especially important since it has specific forward and aft limits that affect its stability and control. As discussed in §11.3, the neutral point of the aircraft falls at 23.6%

MAC, and the flap center of pressure is at 8.25% MAC. Thus, the CG must lie between these points, optimally near the middle between these points, for the aircraft to be sufficiently stable and trimmable. As shown in Figure 18.2-1, the Boomerang only experiences a CG travel of less than 5% MAC.

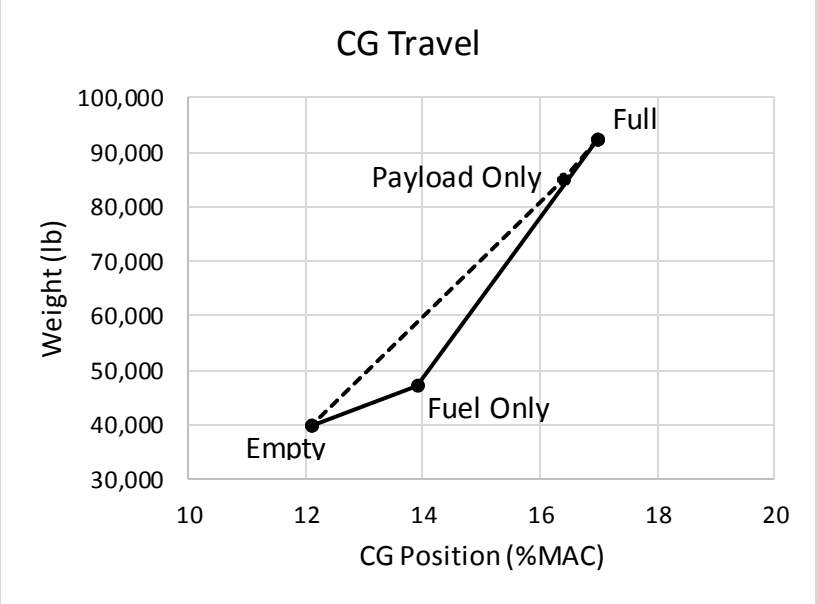

Table 18.1-1: CG travel of less than 5% MAC

19.0 Stability and Trim

Nicolai and Carichner [8] lists several stability derivative requirements that must be met in order to satisfy MIL-HDBK-1797 stability and control requirements and handling qualities. Each one is addressed in the following sections. To determine the stability derivatives, Roskam [15] and Nelson [20] were used.

19.1 Stability Derivatives

19.1.1 Longitudinal Stability, C_{M_α}

For positive longitudinal stability, the change in pitching moment due to angle of attack, C_{M_α}, must be negative. Additionally, C_M must be positive at 0° angle of attack. Since the Boomerang is tailless, only the wing pitching moments are included in this analysis. In a clean configuration, XFLR5 was used to calculate the 0° angle of attack pitching moment coefficient, which was found to be 0.012. With no horizontal tail involved, the value for C_{M_α} is simple and presented in Equation 19.1.1-1.

$$C_{M_\alpha} = -\frac{x_w}{\bar{c}}\left(C_{L_\alpha}\right)_w \qquad \text{Eq. 19.1.1-1}$$

Where $x_w/\bar{c}$ is the static margin and $\left(C_{L_\alpha}\right)_w$ is the lift curve slope of the wing. In the most aft CG case, the static margin is 6.6%, and the value for C_{M_α} is -0.27 per radian, an acceptable value.

19.1.2 Directional Stability, C_{n_β}

To be directionally stable, the variation of yawing moment with sideslip derivative, C_{n_β}, must be positive. As part of the tail sizing analysis in §13.1 and 13.2, C_{n_β} was determined using the methods of Nelson taking into account both the wing and fuselage contribution and the vertical tail contribution and was found to be 0.090 per radian, a positive value in line with historical aircraft.

19.1.3 Roll Damping Derivative, C_{l_p}

In order to meet the roll handling requirements, the roll damping derivative, C_{l_p}, must be negative. This derivative is affected by the wing, horizontal tail, and vertical tail, but of course the horizontal tail contribution was neglected for the Boomerang. Using the methods in Roskam, the derivative was found to be -0.422 per radian, a negative value well aligned with historical aircraft.

19.1.4 Pitch Damping Derivative, C_{M_q}

To meet short-period damping requirements, the pitch damping derivative, C_{M_q}, must be negative. This derivative is also affected by both the wing and horizontal tail, so only the wing is relevant for the Boomerang. Again using Roskam, the value was found to be -2.7 per radian. Though this value is only 10-25% as large as traditional aircraft, NACA TN837 explains that the actual damping of oscillations in flight are nearly as great for a tailless configuration. For a

statically stable tailless aircraft, the rotations in pitch are coupled with vertical motion and provide the satisfactory short-period oscillation mode damping.

19.1.5 Rolling Stability and Dihedral Effect, C_{l_β}

In order to be stable in roll and keep the spiral mode from being divergent, the variation of rolling moment with sideslip, C_{l_β}, must be negative. It should not be too negative, however, or else the aircraft can be sluggish and hard to roll effectively. This derivative is affected by a number of parameters including the wing dihedral angle, vertical location of the wing on the fuselage, wing sweep, and also a vertical tail contribution. The moderate sweep and high wing location of the Boomerang contribute to a significantly negative value of C_{l_β}. With no dihedral, the value is -0.40 per radian, which is 3-4 times the value of most aircraft. Thus, significant anhedral of -7°, comparable to the An-124 and An-225, is required to bring the value to -0.26, a value still lower than optimal, but more acceptable.

19.1.6 Stability Derivative Summary

Table 19.1.6-1 summarizes the values of the stability derivatives along with the requirements and typical values.

Table 19.1.6: Stability derivative summary

Derivative	Requirement	Typical Values (per radian)	Boomerang Value (per radian)
C_{M_α}	< 0	-1.5 – -0.1	-0.27
C_{n_β}	> 0	0.05 – 0.3	0.09
C_{l_p}	< 0	-0.3 – -0.5	-.422
C_{M_q}	< 0	-10 – -25	-2.7
C_{l_β}	< 0	-0.05 – -0.15	-0.26

19.2 Inboard Flap Trimming

As discussed in §11.2, downward deflections of the inboard flap are used to trim the aircraft in flight instead of deflections of the outboard wing. With the center of pressure of the flap ahead of the aircraft CG, these downward deflections cause a positive nose-up pitching moment. As the nose pitches up, the increased wing lift due to the angle of attack reduces the pitching moment until the aircraft is trimmed at a higher angle of attack and its correspondingly higher lift coefficient. Thus, for any flap deflection, assuming no concurrent elevon deflection,

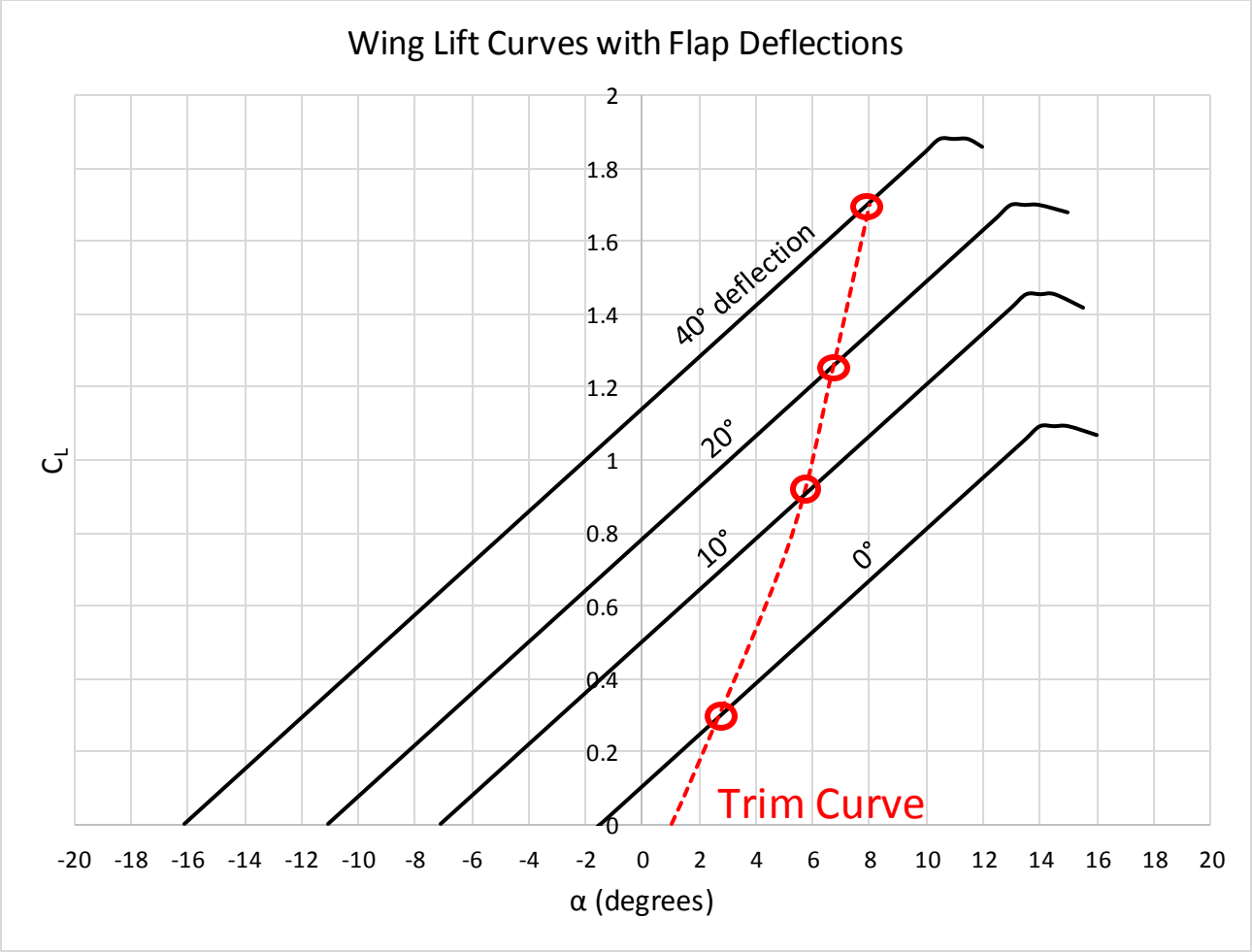

Figure 19.2-1: Trim at various flap setting and no elevon deflection

each flap setting trims the aircraft to a specific angle of attack. XFLR5 was used to determine the trim angle of attack for various flap deflection angles, shown in Figure 19.2-1. For a particular flap deflection, the angle of attack was varied until the overall pitching moment reaches 0.

Recalling that the optimum cruise lift coefficient is 0.68, the aircraft is trimmed at approximately 5° angle of attack and a flap deflection of about 5°. This flap deflection causes a trim drag coefficient of 0.00045, only a 2.7% increase in drag during cruise from a purely clean configuration, an excellent value for trim drag.

19.2.1 Wing Incidence Angle

In order to keep the aircraft roughly level during flight, a wing incidence angle of 4° was chosen. When fully loaded, even at the lower, slower cruise, the cruise C_L is in the 0.6-0.7 range. However, when empty on a ferry flight, the cruise C_L can drop to around 0.4. Thus, 4° incidence provides a good compromise between various loading conditions so that the fuselage can remain level.

20.0 Payload-Range Diagram

Using Torenbeek's methods in [18] range curves were constructed using a fuel capacity of 7,500 lb. At optimum cruise conditions with a full payload, the Boomerang can fly 1,090 nm; this allows the aircraft to meet the range requirements in the case of non-optimal conditions such as a headwind. In a no-payload ferry condition, the range is increased to 2,320 nm.

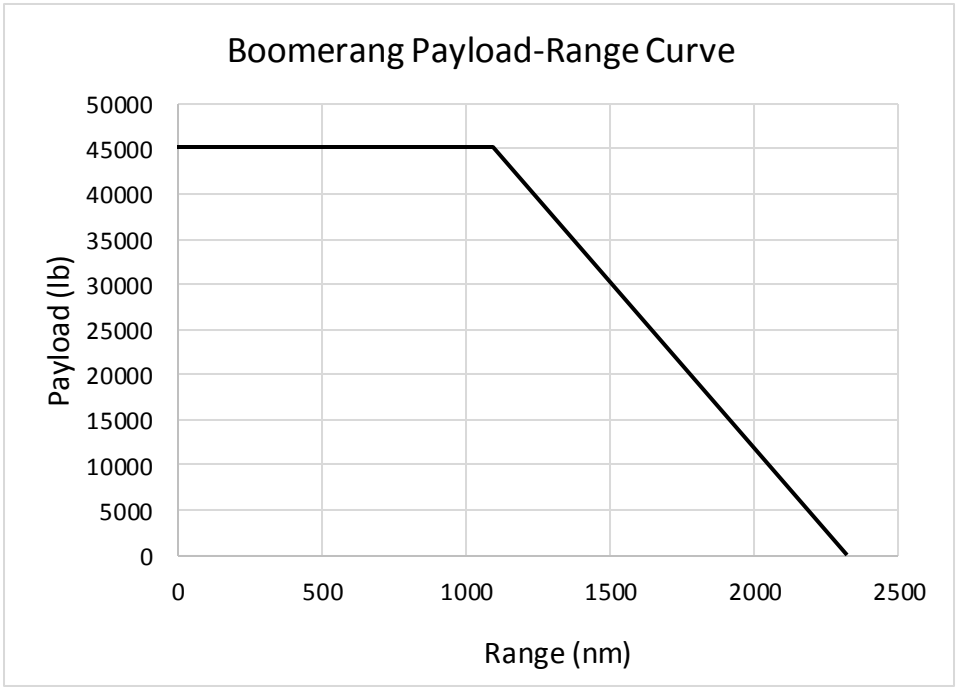

Figure 20.0-1: Boomerang payload-range curve

21.0 Takeoff and Landing Lengths

From the RFP requirements, the aircraft must be able to take off and land in 3,500 ft or less. Takeoff and landing were assumed to take place at sea level standard day conditions.

21.1 Balanced Field Length

The takeoff length is the longer of the nominal takeoff distance and the balanced field length. Using Nicolai and Carichner [8], the nominal takeoff distance was found to be 3,400 ft, just under the RFP requirement. Using the requirements of MIL-C-005011B, the critical or balanced field length is the total runway length needed with an engine failure at the critical point during the takeoff acceleration that stopping the aircraft or continuing the takeoff would require the same amount of runway. This distance also takes into account the distance required to clear a 50 ft obstacle after liftoff. After the critical engine failure, it is assumed that the pilot takes 3 seconds to react, so the aircraft continues to accelerate during this time. While on the ground, the aircraft is also assumed to be in ground effect. Other assumptions include a rolling coefficient of

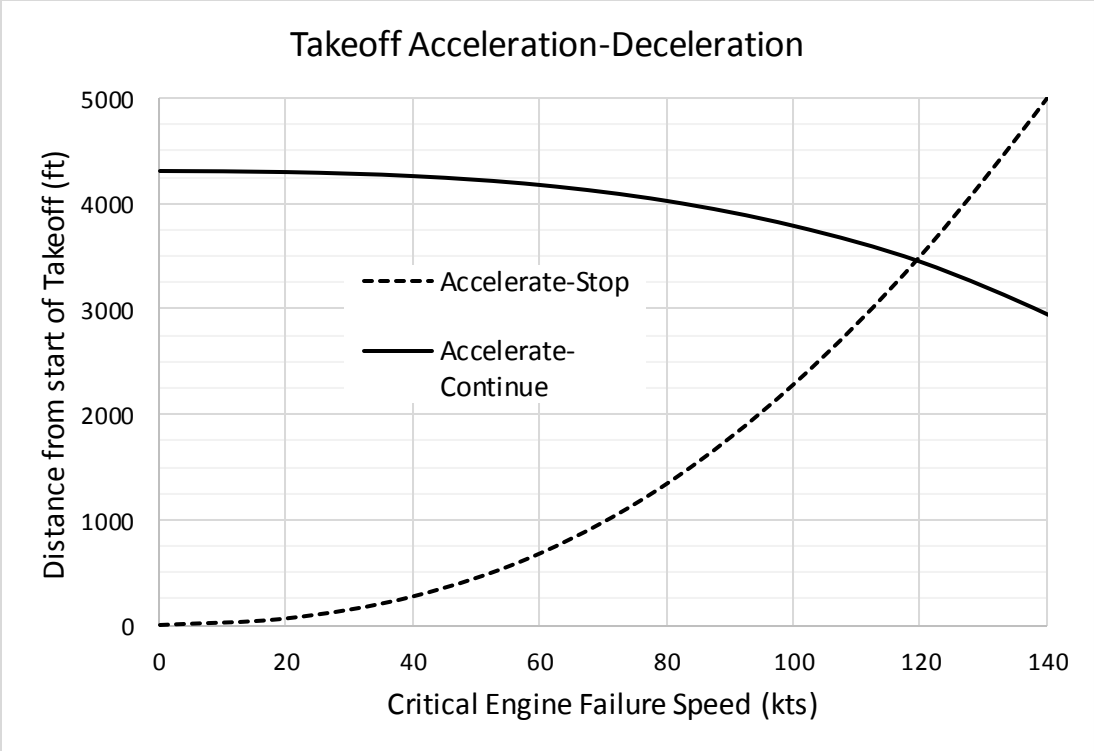

Figure 21.1-1: Balanced field length

0.025 and a braking friction coefficient of 0.30. Figure 21.1-1 shows that the critical engine failure speed is 120 kts, leading to a balanced field length of 3,460 ft, just below the RFP requirements.

21.2 Landing Length

The landing length is the total distance required to cross over a 50 ft obstacle, touch down, and come to a full stop. Using the methods of Nicolai and Carichner [8], the total distance is estimated from the total air distance, free roll distance, and braking distance. The air distance is the distance covered in a constant glide slope. The flair is too imprecise to effectively analyze and is ignored. On touchdown it is assumed that the aircraft rolls freely without significant deceleration for three seconds. Finally, the aircrafts retardation devices such as spoilers and brakes come into effect. A turboprop aircraft like the Boomerang can reverse the propeller pitch so that a retarding force of up to 60% static thrust can be applied throughout the entire braking roll; however, this is ignored for purposes of MIL-C-005011B and the RFP requirements. Table 21.2-1 summarizes the landing distances and compares the braking distance with the addition of reverse thrust. Even without reverse thrust, the Boomerang meets the RFP requirement.

Table 21.2-1: Landing length by segments

Landing Segment	Length (no reverse thrust) (ft)	Length (with reverse thrust) (ft)
Air	1180	1180
Free Roll	560	560
Braking	1630	840
Total	**3370**	**2580**

22.0 Landing Gear and Tires

With a high wing and no load-bearing structure around the payload, the only loacation for the landing gear is in the engine nacelles. Consideration must also be taken to allow the Boomerang to land and operate on rough surfaces, as specified in the RFP. The main criteria for

the landing gear geometry is that is must fit within the angine nacelle, the angle of the gear behind the CG must be greater than 10°, though not so large that the aircraft is difficult to rotate on takeoff, the rollover angle must be less than 63°, and an adequate weight distribution must be placed on the main and nose gear in all loading conditions (approximately 15% of the weight on the nose gear).

22.1 Landing Gear Definition

In order to keep the payload 3 ft above the ground, a gear length of 7.0 ft is required. The engine nacelles are 15 ft from the fuselage centerline, so the wing is 1.84 ft lower then the root at the nacelle attachment point due to anhedral. The engine itself has a diameter of 27 inches, so 30 inches was used to account for clearances. This places the bottom of the engine at 5.5 ft above the bottom of the container's bottom. The main landing gear tire selected in §22.4 has a diameter of 40 inches, so an additional 1.5 ft could be subtracted from the actual gear length necessary, accounting for some deformation of the tires when loaded. A length of 7.0 ft. then provides adequate height to lift the bottom of the container 3 ft from the ground.

22.2 Retraction Scheme

The Boomerang gear retracts much like the DHC-8 shown in Figure 22.0-1 except the the attachment point is in the aft section of the nacelle and retracts forward rather than backward. The aft attachment point was preferred over a forward attachment point on order to maintain adequate gear loads.

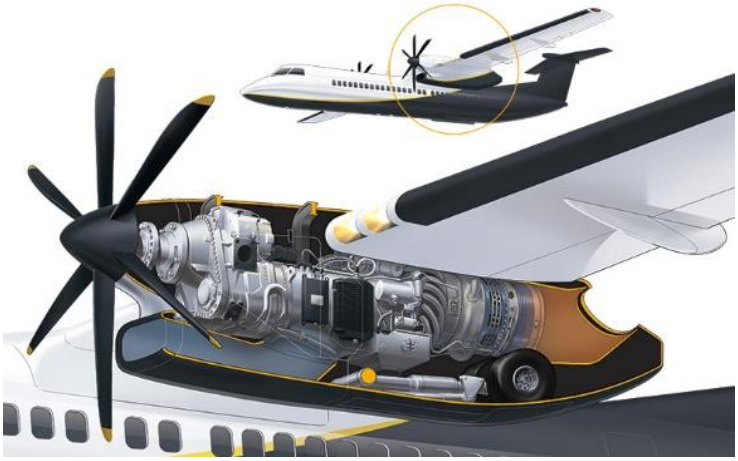

Figure 22.1-1: DHC-8 nacelle landing gear arrangement[8]

[8] https://c1.staticflickr.com/3/2359/2634342194_448f1b9c4a_z.jpg?zz=1

22.3 Gear Loads and Geometry

The nose gear is placed 4 ft aft of the nose in order to maintain adequate loadings in all CG locations. Table 22.3-1 lists the gear loadings for all CG travel.

Table 22.3-1: Nose gear loadings

Loading Condition	W_{MG} (lb)	W_{NG} (lb)	$\%W_{NG}$
Full	79600	12700	13.8
Payload Only	73000	12000	14.0
Ferry	40000	7100	15.1
Empty	33500	6300	15.9

Another geometric constraint on the nose gear is that the tipback angle between the CG and the contact point of the main gear tires be greater than 10°. The Boomerang CG at its highest point is located 8.2 feet above the bottom of the container, thus 11.2 ft above the ground. The tipback angle in this case is 18.6°, greater than the required 10°. As described in Brandt [7], the rollover angle must also be less than 63°. Following the steps to create an auxilliary view of the aircraft's CG, the rollover angle was found to be 44.7°, well within the maximum of 63°, as shown in Figure 22.3-1.

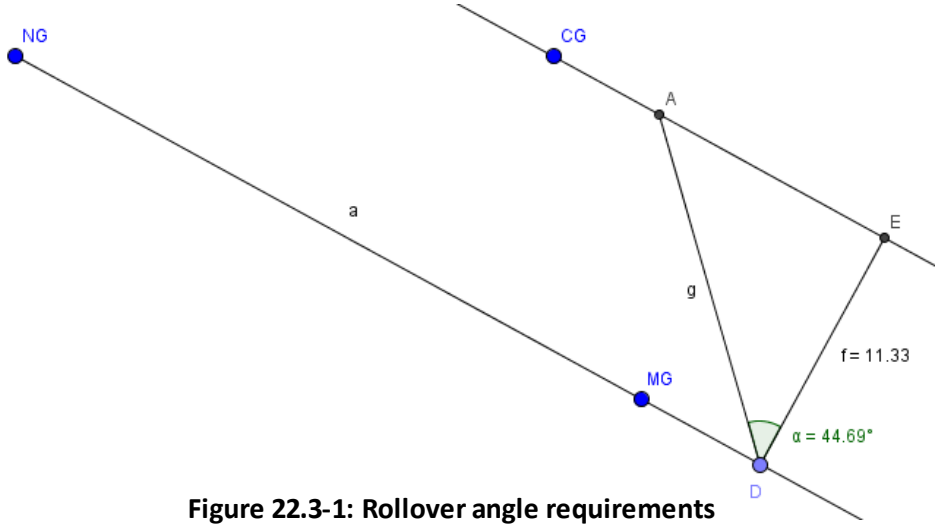

Figure 22.3-1: Rollover angle requirements

22.4 Tire and Rough Field Considerations

In [5], Currey describes a method to determine the flotation (the measure of an aircraft to operate on an airfield of a given strength) of an aircraft operating on a soft field. Recalling §3.3,

California Bearing Ratio (CBR) is a measures of an airfield's surface quality where a lower value correlates with a softer surface. A derived requirement of the Boomerang was to operate out of field with a CBR of 6 or less. A number of factors affect the floatation including the aircraft weight, tire pressure, and tire arrangement. In order to choose a suitable tire for the Boomerang, the the Goodyear Aviation Tire Catalogue [21] was referenced. Tires for the nose and main gear were selected based on diameter, rated load, and rated pressure. For rough field considerations, rated pressure is particularly important. For the Boomerang, an actaual pressure of about 100 psi was ideal. To determine the actual tire pressure, the ratio of the actual load to the rated load was multiplied by the max allowable pressure. For the main gear, two 40 inch diameter Goodyear H40x14.5-19 tires per gear strut were selected, the same tire used on the Boeing 737-200, known for operating out of rough fields, particularly in Alaska. For the nose gear, two 25.5 inch diameter 25.5x8.75-10 tires were selected, used on the main gear of the Dornier Do-228 and Do-328.

Following Currey's methods, the final output is the allowable number of passes (one landing or one takeoff) the nose gear and main gear can make over a field of given CBR. The lower of the two is the final allowable number of passes. This is all summarized in Table 22.4-1. As this shown, the Boomerang main gear is the more limiting than the nose gear and can make over

Table 22.4-1: Tire and flotation details

	Main Gear	Nose Gear
Tire Designation	H40x14.5-19	25.5x8.75-10
Diameter (in)	40	25.5
Width (in)	14.5	8.75
Rated Load (lb)	33,200	8,500
Rated Pressure (psi)	200	101
Actual Max Load (lb)	20,000	6,400
Actual Max Pressure (psi)	120	76
Passes Allowable, CBR = 6	510	>1000
Passes Allowable, CBR = 4	45	88

500 passes on a field with a CBR of 6 and up to 45 passes on a field with a CBR of 4. Thus, the Boomerang satisfies the RFP requirement of rough field operations.

23.0 Payload Handling System

To load and unload the payload effectively, a self-contained payload handling system is included in the Boomerang. It is comprised of a 20 ft container spreader, a pair of 2 HP electric motors, a large lithium-ion battery to power the motors, and a pair of 35 ton jackscrews connecting the motors to the spreader.

23.1 Batteries vs. APU

Compared to an auxiliary power unit (APU), a large capacity lithium-ion battery offers significant weight savings since payload loading and unloading is the main power draw for this system. For example, the Honeywell 131 series APU weighs 361 lb whereas the lithium-ion batteries found in the Boeing 787 weight only 63 lb each. Even with a DC-to-DC converter to adjust the voltage, the battery still comes in much lighter.

23.2 Electric Motor and Battery System

The battery used would be very similar to the battery used by the Boeing 787. This battery weighs 63 pounds and puts out 32 volts at a maximum of 150 amps. The battery is recharged by a generator connected to each engine. The voltage could then be transformed up to 180 volts, the typical input voltage for a 2 HP motor. Ideally, a pair of two motors would draw less than 100 amps from the battery, but even with some degree of inefficiency, this is well below the 150 amp rating. With a capacity of 2,000 Watt-hours, this battery could raise and lower the container over 25 times without needing to be recharged. Thus, a great deal of excess capacity is available for other systems. An example of a suitable motor is the IronHorse MTPM-002-1M18 [22] 2 HP, 180 volt motor, each weighing 62 lb. The total weight of the batteries and

motors would be 187 pounds, which was rounded to 200 lb in the detailed weight breakdown. These motors would each be connected to a 35 ton steel jackscrew such as the Joyce/Dayton WJ3235 [23]. A strength of 35 tons provides enough strength for the fully loaded container to be secure during all maneuvers covered in the V-n diagram, most notably the maximum load factor of 3. This jackscrew has a diameter of 3 ¾" with a worm gear ratio of 32:1. With the electric motors operating at full power, a fully loaded container could be lifted 3 ft from ground level in just over one minute.

23.3 Container Spreader

The vital link between the aircraft and the container itself is the spreader. The spreader used would be similar to that shown in Figure 23.3-1. Instead of the locking mechanism controlled by the suspension cables, however, a small electric motor in the center can activate the twistlocks on each corner simultaneously. A 20 ft steel spreader such as the Timars C-lift weighs approximately 2,000 lb. The twistlocks in each corner, as shown in Figure 23.3-2, have a tensile load rating of 25,000 kg (55,116 lb) slide into the corner castings of the container and then rotate to lock it into place. As discussed in §5.2, the container is also rated at 25 tonnes on each corner. This is more than enough for the maximum load factor of 3 to keep the container secured.

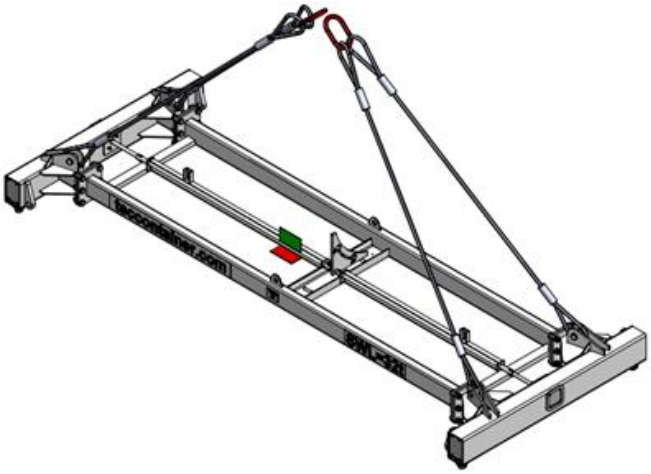

Figure 23.3-1: Typical container spreader[9]

Figure 23.3-2: Twistlock example [24]

[9] http://www.greenfieldpi.com/assets/17/19/DimRegular/TC20_Spreader_IMG.PNG

24.0 Subsystems

With excess battery capacity available, several subsystems can be reconfigured to electric power, for both weight and maintenance savings.

24.1 Environmental Control and Pneumatic Systems

Traditionally, the aircraft pneumatic and environmental control systems are fed by engine bleed air. As discussed in *Aero Quarterly* [25], the 787 has eliminated bleed air and instead electrically driven compressors provide cabin air and other pneumatic needs. With both engine generators and excess battery capacity, the Boomerang is also eliminating engine bleed air in favor of electric power. Boeing estimates that eliminating the bleed air increases fuel efficiency by approximately 3% and also saves maintenance cost on the bleed air system.

24.2 Hydraulics and Control Surface Actuators

Though electromechanical actuators have been successfully tested, as on the NASA F/A-18B [26], they have yet to attain widespread use and acceptance. Hydraulic systems are still standard on modern aircraft. Though the Boeing 787 continues to use a hydraulic system, it replaces the air-turbine-driven hydraulic pumps of the center hydraulic system with electric-motor-driven pumps, which saves both space and weight [25]. The Boomerang emulates 787 with three independent hydraulic systems, left, center, and right, all driven by electric pumps.

25.0 Final Cost Analysis

The same methods as §9.0 were redone for the final Boomerang configuration. With decreased weight and fuel burn, reduced costs from the initial estimates are realized. As before, year 2030 dollars are assumed as well as one test and development aircraft followed by 150 production

Table 25.0-1: Development and production costs

Cost	
Development	$880M
Total Production	$6.0B
Flyaway	$40M
Unit Break-Even	$46M
Selling Price	$50M

aircraft. The selling price assumes a 10% profit on top of the break-even price. These costs are summarized in Table 25.0-1. The direct operating costs are similarly summarized in Table 25.0-2. An additional benefit of the fast cruise speed is that the mission block time is reduced, reducing crew and maintenance costs per flight.

Table 25.0-2: Mission direct operating cost

Cost	
Fuel	$8,850
Crew	$4,180
Maintenance	$10,100
Total	$23,130

By comparison a C-130J cost $48.5 million in 1998, which corresponds to $129 million 2030 dollars. Also, a 1,000 nm mission in a C-130J, using the *Defense News* [27] figure of $9,111 per hour (2012 dollars) would cost $50,000-$55,000 (2030 dollars) depending exactly how long the mission block time is. Thus, the Boomerang is not only less expensive to acquire but also less expensive to operate than a C-130J, a comparable aircraft.

26.0 Summary

The Boomerang meets all requirements provided by the RFP at a very competitive cost to alternative aircraft. Through the use of a novel configuration inspired by the Swift glider, the Boomerang eliminates the need for excess fuselage volume and overly large tail surfaces. It also incorporates modern technological advances such as composite materials, power-dense lithium-ion batteries, and electric pneumatic control. The Boomerang opens up new missions previously not possible with traditional aircraft. Though other aircraft may be able to carry a 20 ft shipping container, none can do it with the turnaround speed afforded by the Boomerang.

Works Cited

[1] "CONTAINER AIRCRAFT LOADING." *CONTAINER AIRCRAFT LOADING*. CDK Mobile Systems, Inc., n.d. Web. 01 May 2016.

[2] United States. Air Force. *MIL-C-005011B*. N.p.: n.p., 1977. Print.

[3] Evans, Stanley H. "Cargo-Carrier Concept." *Flight* 21 Sept. 1950: 331-33. Web.

[4] Kroo, Ilan. "Design and Development of the SWIFT - A Foot-launched Sailplane." *18th Applied Aerodynamics Conference* (2000): n. pag. Web.

[5] Currey, Norman S. *Aircraft Landing Gear Design: Principles and Practices*. Washington, D.C.: American Institute of Aeronautics and Astronautics, 1988. Print.

[6] Jones, Robert T. *Notes on the Stability and Control of Tailless Airplanes*. Tech. no. TN837. Washington: National Advisory Committee for Aeronautics, 1941. Print.

[7] Brandt, Steven A. *Introduction to Aeronautics: A Design Perspective*. Reston, VA: American Institute of Aeronautics and Astronautics, 1997. Print.

[8] Nicolai, Leland M., and Grant Carichner. *Fundamentals of Aircraft and Airship Design*. Reston, VA: American Institute of Aeronautics and Astronautics, 2010. Print.

[9] Murdoch, Eric, Charles Taylor, and David Tozer. A Master's Guide to Container Securing. 2nd ed. N.p.: Standard P&I Club, 2012. Web.

[10] Sforza, Pasquale M. *Commercial Airplane Design Principles*. Waltham: Butterworth-Heinemann, 2014. Print.

[11] "Airfoil Tools." Airfoil Tools. AirfoilTools.com, n.d. Web.

[12] El-Sayed, Ahmed F. *Aircraft Propulsion and Gas Turbine Engines*. Boca Raton: CRC, 2008. Print.

[13] Anderson, John D. *Aircraft Performance and Design*. Boston: WCB/McGraw-Hill, 1999. Print.

[14] "Why Starship 1 Uses P&W Power." *Flight International* 22 Oct. 1983: 1115. Print.

[15] Roskam, Jan. *Methods for Estimating Stability and Control Derivatives of Conventional Subsonic Airplanes*. Lawrence: U of Kansas, 1971. Print.

[16] Sadraey, Mohammad H. *Aircraft Design - A Systems Engineering Approach*. N.p.: Wiley, 2013. Print.

[17] Nita, M., and D. Scholz. "Estimating the Oswald Factor from Basic Aircraft Geometrical Parameters." *Deutscher Luft- Und Raumfahrtkongress* (2012): n. pag. Web.

[18] Torenbeek, Egbert. *Optimum Cruise Performance of Subsonic Transport Aircraft*. Delft, Netherlands: Delft UP, 1998. Print.

[19] Roskam, Jan. *Airplane Design*. Ottawa, Kan.: Roskam Aviation and Engineering, 1985. Print.

[20] Nelson, Robert C. *Flight Stability and Automatic Control*. New York: McGraw-Hill, 1989. Print.

[21] Goodyear Aviation Tires. Akron: Goodyear Aviation, 2015. Print.

[22] IronHorse® Permanent-Magnet DC Motors (SCR Rated) Model Overview. N.p.: Automation Direct, 2014. Web.

[23] Joyce Dayton. MACHINE SCREW JACKS. Kettering: Joyce Dayton, n.d. Web.

[24] William Cook Intermodal. Twistlocks for The Transport Industry. Stanhope Co Durham: William Cook Intermodal, n.d. Web.

[25] Sinnett, Mike. "787 No-Bleed Systems: Saving Fuel and Enhancing Operational Efficiencies." *Aero Quarterly* 2007: 6-11. Web. 16 Apr. 2016.

[26] Jensen, S.c., G.d. Jenney, and D. Dawson. "Flight Test Experience with an Electromechanical Actuator on the F-18 Systems Research Aircraft." 19th DASC. *19th Digital Avionics Systems Conference. Proceedings (Cat. No.00CH37126)* (2000): n. pag. Web.

[27] Weisgerber, Marcus. "USAF: We Didn't Inflate C-27J Costs." *Defense News*. N.p., 27 Mar. 2012. Web. 3 Apr. 2016.

Other Works not Explicitly Referenced in the Text

B.H. Little, Jr. "Propulsion System Installation Design for High-Speed Prop-Fans." *Journal of Aircraft* 20.5 (1983): 411-17. Microform.

Colgren, R., and R. Loschke. "Effective Design of Highly Maneuverable Tailless Aircraft." *Journal of Aircraft* 45.4 (2008): 1441-449. Web.

Conway, Hugh Graham. *Landing Gear Design*. London: Chapman & Hall, 1958. Print.

Hager, Roy D., and Deborah Vrabel. *Advanced Turboprop Project*. Washington, DC: Scientific and Technical Information Division, National Aeronautics and Space Administration, 1988. Print.

Lee, Russell. *Only the Wing: Reimar Horten's Epic Quest to Stabilize and Control the All-wing Aircraft*. Washington, D.C.: Smithsonian Institution Scholarly, 2011. Print.

Maloney, Edward T., and Donald W. Thorpe. *Northrop Flying Wings*. Buena Park, CA: World War II Publications, 1975. Print.

Martinez-Val, R., E. Perez, J. Puertas, and J. Roa. "Optimization of Planform and Cruise Conditions of a Transport Flying Wing." *Proceedings of the Institution of Mechanical Engineers, Part G: Journal of Aerospace Engineering* 224.12 (2010): 1243-251. Web.

"NORTHROP XB-35/YB-35." *Northrop XB-35/YB-35 - Avionslegendaires.net*. N.p., 4 Dec. 2013. Web. 1 May 2016.

Pamadi, Bandu N. *Performance, Stability, Dynamics, and Control of Airplanes*. Reston, VA: American Institute of Aeronautics and Astronautics, 1998. Print.

Raymer, Daniel P. "A Tale of No Tail." *Aerospace America* 5 Nov. 2012: 34. Web.

Reed, Arthur. *C-130 Hercules*. London: Ian Allan, 1984. Print.

Torenbeek, Egbert. *Advanced Aircraft Design: Conceptual Design, Technology and Optimization of Subsonic Civil Airplanes*. West Sussex: Chichester, 2013. Print.

Vecchia, Pierluigi Della, and Fabrizio Nicolosi. "Aerodynamic Guidelines in the Design and Optimization of New Regional Turboprop Aircraft." *Aerospace Science and Technology* 38 (2014): 88-104. Web.

Wainfan, Barnaby, and Hans Nieubert. *Feasibility Study of the Low Aspect Ratio All-Lifting Configuration as a Low-Cost Personal Aircraft*. Tech. no. NAG-1-03054. Hampton: NASA Langley Research Center, 2004. Web.

Wooldridge, E. T. *Winged Wonders: The Story of the Flying Wings*. Washington, D.C.: Published for the National Air and Space Museum by the Smithsonian Institution, 1983. Print.